

AN ASYMPTOTIC PRESERVING AND ENERGY STABLE SCHEME FOR THE BAROTROPIC EULER SYSTEM IN THE INCOMPRESSIBLE LIMIT

K. R. ARUN, RAHULDEV GHORAI, AND MAINAK KAR

ABSTRACT. An asymptotic preserving and energy stable scheme for the barotropic Euler system under the low Mach number scaling is designed and analysed. A velocity shift proportional to the pressure gradient is introduced in the convective fluxes, which leads to the dissipation of mechanical energy and the entropy stability at all Mach numbers. The resolution of the semi-implicit in time and upwind finite volume in space fully-discrete scheme involves two steps: the solution of an elliptic problem for the density and an explicit evaluation for the velocity. The proposed scheme possesses several physically relevant attributes, such as the positivity of density, the entropy stability and the consistency with the weak formulation of the continuous Euler system. The AP property of the scheme, i.e. the boundedness of the mesh parameters with respect to the Mach number and its consistency with the incompressible limit system, is shown rigorously. The results of extensive case studies are presented to substantiate the robustness and efficiency of the proposed method.

1. INTRODUCTION

Mechanical processes acting on different spatial and temporal scales are quite common in many applications in physics, engineering and industry. Compressible fluid flow problems modelled by the Euler equations often give rise to such multiscale phenomena. At room temperatures, pressure pulses travel at a speed of about 343 meters per second whereas a typical fluid motion under such conditions is usually for about 10 meters per second. In other words, there can exist two different velocity scales within the same physical problem and this apparent disparity in the wave-speeds is usually quantified using the Mach number which is the ratio of convection velocity to the sound velocity. From a mathematical point of view, the hydrodynamics at low Mach numbers merits a careful attention. It has been well established that solutions of the compressible Euler equations converge to their incompressible counterparts when the Mach number goes to zero; see e.g. [43, 54]. In the mathematical literature, the zero Mach number limit is often treated as a singular limit under which the purely hyperbolic compressible Euler system changes its nature to the mixed hyperbolic-elliptic incompressible Euler system; see [46] and the references therein for a rigorous treatment.

Since the zero Mach number limit is singular for the compressible Euler equations, classical explicit time-stepping methods designed for hyperbolic conservation laws are inadequate for low Mach number computations. Indeed, explicit schemes are known to exhibit severe pathologies when used to simulate low Mach number flows; see [44] for a review. The difficulties associated with the numerical solution of Euler equations at low Mach numbers are numerous. Due to the large discrepancy between the fluid and sound velocities, the CFL condition imposes an acute restriction on the time-step to maintain stability and this in turn contributes to stiffness and prohibitive computational costs. One of the early attempts in this direction to circumvent the stiffness by

Date: July 21, 2023.

2010 Mathematics Subject Classification. Primary 35L45, 35L60, 35L65, 35L67; Secondary 65M06, 65M08.

Key words and phrases. Compressible Euler system, Incompressible limit, Asymptotic preserving, Finite volume method, MAC grid, Entropy stability.

K. R. A. gratefully acknowledges Core Research Grant - CRG/2021/004078 from Science and Engineering Research Board, Department of Science & Technology, Government of India.

using semi-implicit schemes for low Mach number hydrodynamics is available in [48, 53]. Extension of these ideas to high orders and their implementation on general unstructured meshes can be found in [4, 9, 10, 56]. If the numerical viscosity introduced by upwind discretisations depends on the Mach number, then it can ultimately lead to instabilities or inconsistent numerical solutions; see e.g. [33] for more details. Furthermore, it has been also reported that the presence of spurious acoustic waves can deteriorate the order of accuracy of Godunov-type explicit finite volume schemes at low Mach numbers; see [1, 3, 18].

An effective platform to design robust numerical approximations for the low Mach number Euler equations, or singularly perturbed hydrodynamic models of fluids in general, is the so-called ‘Asymptotic Preserving’ (AP) methodology which was introduced in the context of kinetic models of diffusive transport [41]. AP schemes provide a general framework to numerically tackle any singular perturbation problem and their working principle can be explained as follows. Let \mathcal{P}_ε denote a singularly perturbed problem with ε , the perturbation parameter. Suppose that in the limit as $\varepsilon \rightarrow 0$, the solution of \mathcal{P}_ε converges to the solution of a well-posed problem denoted by \mathcal{P}_0 , called the singular limit or the limit problem. A numerical scheme for \mathcal{P}_ε , denoted by $\mathcal{P}_\varepsilon^h$ with h being a discretisation parameter, is said to be AP if

- (i) as $\varepsilon \rightarrow 0$ the numerical scheme $\mathcal{P}_\varepsilon^h$ converges to a numerical scheme \mathcal{P}_0^h , which is a consistent discretisation of the limit system \mathcal{P}_0 and
- (ii) the stability constraints on the discretisation parameter h are independent of ε .

Therefore, the AP methodology turns out to be a natural choice for the numerical approximation of the zero Mach number limit in the sense that it respects the limit at a discrete level. Furthermore, the AP framework automatically recognises the singular (weakly compressible or nearly incompressible) and non-singular (compressible) regions in the flow as well as the transient regions where regime shifts take place. Thus, using an AP discretisation for low Mach number flows is an effective method that drastically reduces the computational complexity while simultaneously enhancing the accuracy.

A common practice to design AP schemes for hydrodynamic models, such as the Euler equations, is to employ an implicit-explicit (IMEX) time discretisation. We refer the reader to [2, 3, 6, 7, 8, 11, 16, 34, 39, 50, 57] for some developments on IMEX AP schemes for stiff hydrodynamic problems. The IMEX time-stepping procedure relies on a stiff/non-stiff splitting of the fluxes and subsequently, the stiff terms are treated implicitly and the non-stiff terms explicitly. The semi-implicit formalism has the advantage that it avoids the need to invert large and dense matrices, typical of fully-implicit schemes, at the same time it overcomes the restrictive stability conditions of fully-explicit schemes. In the case of the barotropic Euler equations, a semi-implicit AP scheme necessitates the implicit treatment of the mass flux and the pressure gradient in the momentum flux [3, 8, 16]. A reformulation of the resulting scheme can be performed, nonetheless, to yield an elliptic equation for the pressure which is nothing but the time discretisation of a wave equation for the pressure in the continuous case. However, the discrete diffusion operator in the above elliptic problem, arising by combining discrete gradient and divergence operators, does not satisfy the so-called ‘inf-sup’ condition. As a result, the scheme might require an additional stabilisation procedure at low Mach numbers [47]. A possible cure to this ailment is to extend the standard, well-established discretisation techniques of incompressible flows to the compressible case. A first attempt in this direction can be found in [35] which can be seen as an extension of the well-known ‘Marker and Cell’ (MAC) scheme [36]. We refer the interested reader to [5, 14, 40, 42, 45, 59] for related treatments. Yet another demand while dealing with the numerical approximation of hyperbolic models of compressible fluids is to maintain the entropy stability. Since the solutions are known to develop discontinuities in finite time, the entropy inequalities are vital in choosing the physically valid weak solutions. Obtaining entropy stable schemes, though nontrivial, is mandatory

in applications, such as the low Mach number hydrodynamics, to derive energy estimates and to perform rigorous asymptotic convergence analysis.

The goal of the present work is the design and analysis of an AP, semi-implicit and entropy stable scheme for the barotropic Euler system on a MAC grid. The key to entropy stability is the introduction of a shifted velocity in the convective fluxes of mass and momenta, following the ideas introduced in [15, 20, 21, 32, 52]. The velocity shift is proportional to the stiff pressure gradient, it stabilises the flow via the dissipation of mechanical energy at all Mach numbers, and the parameters involved in it have to respect a CFL-type condition. The present scheme is closely related to the so-called non-incremental projection scheme due to Chorin [12]. A semi-implicit time discretisation is performed to overcome stiff stability restrictions. The upwind space discretised fully-discrete scheme satisfies the required apriori entropy stability inequalities as in the continuous model. The velocity stabilised mass update gives rise to a well-posed, semilinear elliptic problem for the pressure, thanks to the MAC grid discretisation. After the resolution of the elliptic problem, the momentum update can be evaluated explicitly. We carry out a mathematical and numerical analysis of the proposed scheme that is motivated to an extent by an analogous analysis performed for the prediction-correction semi-implicit scheme in [39]. However, the key differences are that the semi-implicit scheme of [39] is multi-step and it requires an almost well-prepared initial datum to obtain the AP property. For the present velocity stabilised semi-implicit scheme, the existence of the numerical solution and the positivity of the mass density are established by exploiting some topological degree theory results. A weak consistency analysis of the numerical scheme is performed to establish its consistency with the weak formulation of the Euler equations. A sufficient condition to enforce the stability restriction shows the scheme's ability to admit large time-steps in low Mach number regimes. The AP property of the scheme, i.e. the boundedness of the time-steps with respect to the Mach number and the consistency of the scheme with the incompressible limit, is shown rigorously and numerically by means of extensive case studies.

The rest of this paper is organised as follows. In Section 2 we recall some apriori energy stability estimates that are crucial to establish the incompressible limit and the velocity stabilisation technique based on the energy stability. The discretisation of the domain and the discrete differential operators are introduced in Section 3. The semi-implicit numerical scheme and its energy stability attributes are presented in Section 4. In Section 5 we present the weak consistency results and in Section 6, the asymptotic consistency with the incompressible Euler system. The results of numerical case studies are presented in Section 7. Finally, the paper is concluded with some remarks in Section 8.

2. APRIORI ENERGY ESTIMATES AND THE INCOMPRESSIBLE LIMIT

We start with the following initial boundary problem for the compressible Euler system parametrised by the Mach number ε :

$$(2.1) \quad \partial_t \rho^\varepsilon + \operatorname{div}(\rho^\varepsilon \mathbf{u}^\varepsilon) = 0,$$

$$(2.2) \quad \partial_t(\rho^\varepsilon \mathbf{u}^\varepsilon) + \operatorname{div}(\rho^\varepsilon \mathbf{u}^\varepsilon \otimes \mathbf{u}^\varepsilon) + \frac{1}{\varepsilon^2} \nabla p^\varepsilon = 0,$$

$$(2.3) \quad \rho^\varepsilon|_{t=0} = \rho_0^\varepsilon, \quad \mathbf{u}^\varepsilon|_{t=0} = \mathbf{u}_0^\varepsilon, \quad \mathbf{u}^\varepsilon|_{\partial\Omega} = 0,$$

for $(t, \mathbf{x}) \in Q := (0, T) \times \Omega$, where Ω is an open, bounded and connected subset of \mathbb{R}^d , $d \geq 1$. The parameter $\varepsilon \in (0, 1]$, usually known as the reference Mach number, is an infinitesimal and is defined as the ratio of a characteristic fluid velocity to that of a sound velocity. The variables ρ^ε and \mathbf{u}^ε are the density and velocity of the fluid, respectively. The pressure $p^\varepsilon = p(\rho^\varepsilon)$ is assumed to follow a barotropic equation of state $p(\rho) := \rho^\gamma$ with $\gamma \geq 1$ being the ratio of specific heats.

We first review some apriori energy estimates satisfied by the solutions of (2.1)-(2.2), which are needed to perform the incompressible limit $\varepsilon \rightarrow 0$. To this end, we start with the internal energy per unit volume or the so-called Helmholtz function:

$$(2.4) \quad \psi_\gamma(\rho) := \begin{cases} \rho \ln \rho, & \text{if } \gamma = 1, \\ \frac{\rho^\gamma}{\gamma - 1}, & \text{if } \gamma > 1. \end{cases}$$

The internal energy \mathcal{I}_ε and kinetic energy \mathcal{K}_ε of the system (2.1)-(2.2) are defined by

$$(2.5) \quad \mathcal{I}_\varepsilon(t) := \int_\Omega \psi_\gamma(\rho^\varepsilon) d\mathbf{x}, \quad \mathcal{K}_\varepsilon(t) := \int_\Omega \frac{1}{2} \rho^\varepsilon |\mathbf{u}^\varepsilon|^2 d\mathbf{x}.$$

2.1. Apriori Energy Estimates.

Proposition 2.1. *We recall from [39] the following identities satisfied by regular solutions of (2.1)-(2.2).*

(i) *A renormalisation identity:*

$$(2.6) \quad \partial_t \psi_\gamma(\rho^\varepsilon) + \operatorname{div} (\psi_\gamma(\rho^\varepsilon) \mathbf{u}^\varepsilon) + p^\varepsilon \operatorname{div} \mathbf{u}^\varepsilon = 0.$$

(ii) *A positive renormalisation identity:*

$$(2.7) \quad \partial_t \Pi_\gamma(\rho^\varepsilon) + \operatorname{div} (\psi_\gamma(\rho^\varepsilon) - \psi'_\gamma(1)\rho^\varepsilon) \mathbf{u}^\varepsilon + p^\varepsilon \operatorname{div} \mathbf{u}^\varepsilon = 0,$$

where $\Pi_\gamma(\rho) := \psi_\gamma(\rho) - \psi_\gamma(1) - \psi'_\gamma(1)(\rho - 1)$ is the relative internal energy, which is an affine approximation of ψ_γ with respect to the constant state $\rho = 1$.

(iii) *The kinetic energy identity:*

$$(2.8) \quad \partial_t \left(\frac{1}{2} \rho^\varepsilon |\mathbf{u}^\varepsilon|^2 \right) + \operatorname{div} \left(\frac{1}{2} \rho^\varepsilon |\mathbf{u}^\varepsilon|^2 \mathbf{u}^\varepsilon \right) + \frac{1}{\varepsilon^2} \nabla p^\varepsilon \cdot \mathbf{u}^\varepsilon = 0.$$

(iv) *The total energy identity:*

$$(2.9) \quad \partial_t \left(\frac{1}{2} \rho^\varepsilon |\mathbf{u}^\varepsilon|^2 + \frac{1}{\varepsilon^2} \Pi_\gamma(\rho^\varepsilon) \right) + \operatorname{div} \left(\frac{1}{2} \rho^\varepsilon |\mathbf{u}^\varepsilon|^2 + \frac{1}{\varepsilon^2} \psi_\gamma(\rho^\varepsilon) - \frac{1}{\varepsilon^2} \psi'_\gamma(1)\rho^\varepsilon + \frac{1}{\varepsilon^2} p^\varepsilon \right) \mathbf{u}^\varepsilon = 0.$$

Proof. The proof follows from straightforward calculations; see [39] and the references therein. \square

2.2. Incompressible Limit. In this section we introduce the zero Mach number or the incompressible limit of the Euler system (2.1)-(2.2), which is obtained by letting $\varepsilon \rightarrow 0$. In order to perform the above limit, we first introduce the notion of the so-called ‘ill-prepared’ initial data; see [39] for further details and also [18] for some related discussions on the relevance of initial data in carrying out the incompressible limit.

Definition 2.2. An initial datum $(\rho_0^\varepsilon, \mathbf{u}_0^\varepsilon)$ of (2.1)-(2.2) is called ill-prepared if $(\rho_0^\varepsilon, \mathbf{u}_0^\varepsilon) \in L^\infty(\Omega)^{1+d}$ with $\rho_0^\varepsilon > 0$, and satisfy the bound:

$$(2.10) \quad \|\mathbf{u}_0^\varepsilon\|_{L^2(\Omega)^d} + \frac{1}{\varepsilon} \|\rho_0^\varepsilon - 1\|_{L^\infty(\Omega)} \leq C,$$

where $C > 0$ is a constant that does not depend on ε .

Remark 2.3. The estimate (2.10) implies that $\rho_0^\varepsilon - 1 = \mathcal{O}(\varepsilon)$ and that \mathbf{u}_0^ε is uniformly bounded in $L^2(\Omega)^d$ with respect to ε . The so-called ‘well-prepared’ data from the literature, e.g. [43, 54], requires more stringent restrictions, such as $\rho_0^\varepsilon - 1 = \mathcal{O}(\varepsilon^2)$, a uniform bound on \mathbf{u}_0^ε in $H^1(\Omega)^d$ and $\operatorname{div} \mathbf{u}_0^\varepsilon$ be close to zero.

In the subsequent discussions we will assume the existence of a weak solution $(\rho^\varepsilon, \mathbf{u}^\varepsilon) \in L^\infty(Q)^{1+d}$ of (2.1)-(2.2) that satisfies the total entropy inequality:

$$(2.11) \quad \partial_t \left(\frac{1}{2} \rho^\varepsilon |\mathbf{u}^\varepsilon|^2 + \frac{1}{\varepsilon^2} \Pi_\gamma(\rho^\varepsilon) \right) + \operatorname{div} \left(\frac{1}{2} \rho^\varepsilon |\mathbf{u}^\varepsilon|^2 + \frac{1}{\varepsilon^2} \psi_\gamma(\rho^\varepsilon) - \frac{1}{\varepsilon^2} \psi'_\gamma(1) \rho^\varepsilon + \frac{1}{\varepsilon^2} p^\varepsilon \right) \mathbf{u}^\varepsilon \leq 0.$$

Integrating (2.11) over Q and taking into account the homogeneous Dirichlet boundary condition on the velocity, we further obtain that $(\rho^\varepsilon, \mathbf{u}^\varepsilon)$ satisfies the following total entropy estimate:

$$(2.12) \quad \frac{1}{2} \int_\Omega \rho^\varepsilon(t) |\mathbf{u}^\varepsilon(t)|^2 d\mathbf{x} + \frac{1}{\varepsilon^2} \int_\Omega \Pi_\gamma(\rho^\varepsilon(t)) d\mathbf{x} \leq \frac{1}{2} \int_\Omega \rho_0^\varepsilon |\mathbf{u}_0^\varepsilon|^2 d\mathbf{x} + \frac{1}{\varepsilon^2} \int_\Omega \Pi_\gamma(\rho_0^\varepsilon) d\mathbf{x}.$$

The entropy estimate (2.12) yields the convergence of ρ^ε to 1 as ε goes to 0. Precisely, it can be shown that $\rho^\varepsilon \rightarrow 1$ in $L^\infty(0, T; L^r(\Omega))$ for every $r \in [1, \min\{2, \gamma\}]$ and $\mathbf{u}^\varepsilon \overset{*}{\rightharpoonup} \mathbf{U}$ in $L^\infty(0, T; L^2(\Omega)^d)$ as $\varepsilon \rightarrow 0$; see [39, 43, 46] and the references therein for details. Furthermore, $(\pi, \mathbf{U}) \in L^\infty(0, T; L^2(\Omega))^{1+d}$ is a weak solution of the initial value problem

$$(2.13) \quad \operatorname{div} \mathbf{U} = 0,$$

$$(2.14) \quad \partial_t \mathbf{U} + \mathbf{div}(\mathbf{U} \otimes \mathbf{U}) + \nabla \pi = 0,$$

$$(2.15) \quad \mathbf{U}(0, \cdot) = \mathbf{U}_0, \operatorname{div} \mathbf{U}_0 = 0,$$

for $(t, \mathbf{x}) \in Q$, which is formally the incompressible limit of (2.1)-(2.2).

2.3. Velocity Stabilisation. In the following, we introduce a semi-implicit scheme for the system (2.1)-(2.2) and study its stability in the sense of numerical control of total energy. In other words, we aim at obtaining a discrete equivalent of the energy stability (2.9). In order to enforce the energy stability of the numerical solution, we adopt the formalism introduced in [20, 21, 32, 52]. The idea is to apply a stabilisation, therein a shifted velocity is introduced in the mass and momentum fluxes to yield the modified system:

$$(2.16) \quad \partial_t \rho^\varepsilon + \operatorname{div}(\rho^\varepsilon(\mathbf{u}^\varepsilon - \delta \mathbf{u}^\varepsilon)) = 0,$$

$$(2.17) \quad \partial_t(\rho^\varepsilon \mathbf{u}^\varepsilon) + \mathbf{div}(\rho^\varepsilon \mathbf{u}^\varepsilon \otimes (\mathbf{u}^\varepsilon - \delta \mathbf{u}^\varepsilon)) + \frac{1}{\varepsilon^2} \nabla p^\varepsilon = 0.$$

Analogous to Proposition 2.1, one can derive the following apriori estimates for the solutions of the modified system (2.16)-(2.17). The expression for the stabilisation term $\delta \mathbf{u}^\varepsilon$ is determined accordingly from the total energy estimate so that it ensures the entropy stability.

Proposition 2.4. *Regular solutions of (2.16)-(2.17) satisfy the following identities.*

(i) *A renormalisation identity:*

$$(2.18) \quad \partial_t \psi_\gamma(\rho^\varepsilon) + \operatorname{div}(\psi_\gamma(\rho^\varepsilon)(\mathbf{u}^\varepsilon - \delta \mathbf{u}^\varepsilon)) + p^\varepsilon \operatorname{div}(\mathbf{u}^\varepsilon - \delta \mathbf{u}^\varepsilon) = 0.$$

(ii) *A positive renormalisation identity:*

$$(2.19) \quad \partial_t \Pi_\gamma(\rho^\varepsilon) + \operatorname{div}(\psi_\gamma(\rho^\varepsilon) - \psi'_\gamma(1) \rho^\varepsilon)(\mathbf{u}^\varepsilon - \delta \mathbf{u}^\varepsilon) + p^\varepsilon \operatorname{div}(\mathbf{u}^\varepsilon - \delta \mathbf{u}^\varepsilon) = 0.$$

(iii) *The kinetic energy balance:*

$$(2.20) \quad \partial_t \left(\frac{1}{2} \rho^\varepsilon |\mathbf{u}^\varepsilon|^2 \right) + \operatorname{div} \left(\frac{1}{2} \rho^\varepsilon |\mathbf{u}^\varepsilon|^2 (\mathbf{u}^\varepsilon - \delta \mathbf{u}^\varepsilon) \right) + \frac{1}{\varepsilon^2} (\mathbf{u}^\varepsilon - \delta \mathbf{u}^\varepsilon) \cdot \nabla p^\varepsilon = -\frac{1}{\varepsilon^2} \delta \mathbf{u}^\varepsilon \cdot \nabla p^\varepsilon.$$

(iv) *Adding (2.19) and (2.20) yields the entropy balance:*

$$(2.21) \quad \partial_t \left(\frac{1}{\varepsilon^2} \Pi_\gamma(\rho^\varepsilon) + \frac{1}{2} \rho^\varepsilon |\mathbf{u}^\varepsilon|^2 \right) + \operatorname{div} \left(\frac{1}{2} \rho^\varepsilon |\mathbf{u}^\varepsilon|^2 + \frac{1}{\varepsilon^2} \psi_\gamma(\rho^\varepsilon) - \frac{1}{\varepsilon^2} \psi'_\gamma(1) \rho^\varepsilon + \frac{1}{\varepsilon^2} p^\varepsilon \right) (\mathbf{u}^\varepsilon - \delta \mathbf{u}^\varepsilon) = -\frac{1}{\varepsilon^2} \delta \mathbf{u}^\varepsilon \cdot \nabla p^\varepsilon.$$

Proof. The proof is classical and uses straightforward manipulations as in Proposition 2.1. \square

Thus, at the continuous level, we immediately see that if we formally take $\delta \mathbf{u}^\varepsilon = \eta \nabla p^\varepsilon$ with $\eta > 0$, then we get the entropy stability inequality:

$$(2.22) \quad \partial_t \left(\frac{1}{\varepsilon^2} \Pi_\gamma(\rho^\varepsilon) + \frac{1}{2} \rho^\varepsilon |\mathbf{u}^\varepsilon|^2 \right) + \operatorname{div} \left(\frac{1}{2} \rho^\varepsilon |\mathbf{u}^\varepsilon|^2 + \frac{1}{\varepsilon^2} \psi_\gamma(\rho^\varepsilon) - \frac{1}{\varepsilon^2} \psi'_\gamma(1) \rho^\varepsilon + \frac{1}{\varepsilon^2} p^\varepsilon \right) (\mathbf{u}^\varepsilon - \delta \mathbf{u}^\varepsilon) = -\frac{1}{\varepsilon^2} \eta |\nabla p^\varepsilon|^2 \leq 0.$$

In other words, shifting the velocity has a stabilising effect, which ultimately yields the energy stability; see [20, 21, 32, 52]. Consequently, as ε tends to zero, the modified system (2.16)-(2.17) formally converges to the following velocity stabilised incompressible Euler equations:

$$(2.23) \quad \operatorname{div}(\mathbf{u} - \delta \mathbf{u}) = 0,$$

$$(2.24) \quad \partial_t \mathbf{u} + \mathbf{div}(\mathbf{u} \otimes (\mathbf{u} - \delta \mathbf{u})) + \nabla \pi = 0,$$

where π is the formal limit of $\frac{p(\rho^\varepsilon) - 1}{\varepsilon^2}$ and $\delta \mathbf{u} = \eta \nabla \pi$. Motivated by the above, we design a semi-implicit scheme in which the velocity stabilisation introduced via numerical flux functions is the key to achieve nonlinear energy stability. Using the energy estimate, we establish a discrete analogue of the incompressible limit.

3. DOMAIN DISCRETISATION AND DISCRETE DIFFERENTIAL OPERATORS

In order to approximate the velocity stabilised Euler system (2.16)-(2.17) in a finite volume framework, we take a computational space-domain $\Omega \subseteq \mathbb{R}^d$, such that the closure of Ω is the union of closed rectangles ($d = 2$) or closed orthogonal parallelepipeds ($d = 3$).

3.1. Mesh and Unknowns. In the subsequent discussion, we introduce a discretisation of the domain Ω using a marker and cell (MAC) grid and the corresponding discrete function spaces; see [13, 28, 29, 36] for more details. A MAC grid is a pair $\mathcal{T} = (\mathcal{M}, \mathcal{E})$, where \mathcal{M} is called the primal mesh which is a partition of $\bar{\Omega}$ consisting of possibly non-uniform closed rectangles ($d = 2$) or parallelepipeds ($d = 3$) and \mathcal{E} is the collection of all edges of the primal cells. For each $\sigma \in \mathcal{E}$, we construct a dual cell D_σ which is the union of half-portions of the primal cells K and L , where $\sigma = \bar{K} \cap \bar{L}$. Furthermore, we decompose \mathcal{E} as $\mathcal{E} = \cup_{i=1}^d \mathcal{E}^{(i)}$, where $\mathcal{E}^{(i)} = \mathcal{E}_{\text{int}}^{(i)} \cup \mathcal{E}_{\text{ext}}^{(i)}$. Here, $\mathcal{E}_{\text{int}}^{(i)}$ and $\mathcal{E}_{\text{ext}}^{(i)}$ are, respectively, the collection of $d - 1$ dimensional internal and external edges that are orthogonal to the i -th unit vector $e^{(i)}$ of the canonical basis of \mathbb{R}^d . We denote by $\mathcal{E}(K)$, the collection of all edges of $K \in \mathcal{M}$ and $\tilde{\mathcal{E}}(D_\sigma)$, the collection of all edges of the dual cell D_σ . We define the mesh parameter $h = \max\{\operatorname{diam}(K) : K \in \mathcal{M}\}$.

Now, we define a discrete function space $L_{\mathcal{M}}(\Omega) \subset L^\infty(\Omega)$, consisting of scalar valued functions which are piecewise constant on each primal cell $K \in \mathcal{M}$. Analogously, we denote by $\mathbf{H}_{\mathcal{E}}(\Omega) = \prod_{i=1}^d H_{\mathcal{E}}^{(i)}(\Omega)$, the set of vector valued (in \mathbb{R}^d) functions which are constant on each dual cell D_σ and for each $i = 1, 2, \dots, d$. The space of vector valued functions vanishing on the external edges is denoted as $\mathbf{H}_{\mathcal{E},0}(\Omega) = \prod_{i=1}^d H_{\mathcal{E},0}^{(i)}(\Omega)$, where $H_{\mathcal{E},0}^{(i)}(\Omega)$ contains those elements of $H_{\mathcal{E}}^{(i)}(\Omega)$ which vanish on the external edges. For a primal grid function $q \in L_{\mathcal{M}}(\Omega)$, such that $q = \sum_{K \in \mathcal{M}} q_K \mathcal{X}_K$, and for each $\sigma = K|L \in \cup_{i=1}^d \mathcal{E}_{\text{int}}^{(i)}$, the dual average q_{D_σ} of q over D_σ is defined via the relation

$$(3.1) \quad |D_\sigma| q_{D_\sigma} = |D_{\sigma,K}| q_K + |D_{\sigma,L}| q_L.$$

Remark 3.1. The assumption that the dual variables vanish at the boundary is taken only for the sake of simplicity of the following exposition. In a similar setup, we can consider the space of piecewise constant functions on the dual grid, which can be extended to external dual cells in order to implement periodic boundary conditions. In this case, an external dual cell is obtained by adjoining half portions of a primal cell and a fictitious primal cell outside the domain. Furthermore,

the function values on opposite external dual cells are identified. We have implemented periodic boundary conditions in all of the numerical test problems in Section 7.

3.2. Discrete Convection Fluxes and Differential Operators. In this section, we introduce the discrete convection fluxes and discrete differential operators on the functional spaces described above.

Definition 3.2. Assume a discretisation of Ω with a MAC grid $\mathcal{T} = (\mathcal{M}, \mathcal{E})$ and the discrete function spaces as defined above.

- (i) For each $K \in \mathcal{M}$ and $\sigma \in \mathcal{E}(K)$, $\sigma = K|L$, the mass flux $F_{\sigma,K} : L_{\mathcal{M}}(\Omega) \times \mathbf{H}_{\mathcal{E},0}(\Omega) \rightarrow \mathbb{R}$ is defined by the following splitting of the positive and negative components:

$$(3.2) \quad F_{\sigma,K}(\rho, \mathbf{v}) := |\sigma| \{ \rho_K (v_{\sigma,K})^+ + \rho_L (v_{\sigma,K})^- \}, \quad (\rho, \mathbf{v}) \in L_{\mathcal{M}}(\Omega) \times \mathbf{H}_{\mathcal{E},0}(\Omega).$$

Here, $v_{\sigma,K} = v_{\sigma} \mathbf{e}^{(i)} \cdot \boldsymbol{\nu}_{\sigma,K}$, where $\boldsymbol{\nu}_{\sigma,K}$ is the unit vector normal to the edge $\sigma \in \mathcal{E}_{\text{int}}^{(i)}$ in the direction outward to the cell K . Note that in Subsection 2.3, it is the velocity stabilisation which yields the energy stability of the modified Euler system (2.16)-(2.17). Motivated by the same considerations, we introduce the following stabilisation in the discrete setup:

$$(3.3) \quad v_{\sigma}^n = u_{\sigma}^n - \delta u_{\sigma}(\rho^{n+1}), \quad \text{with } \delta u_{\sigma}(\rho^{n+1}) := \frac{\eta \delta t}{\varepsilon^2} (\partial_{\mathcal{E}}^{(i)} p^{n+1})_{\sigma}, \quad \forall 1 \leq i \leq d, \quad \forall \sigma \in \mathcal{E}_{\text{int}}^{(i)},$$

where $\eta > 0$ is a parameter which will be determined later. Clearly, the stabilised velocity $\mathbf{v}_{\sigma} \in \mathbf{H}_{\mathcal{E},0}(\Omega)$ since both the explicit velocity component and the pressure gradient are defined on the dual cells. It will be shown that the implicit treatment of the stabilising pressure gradient term is crucial to get the entropy stability of the numerical scheme. In order to maintain the sign of the split velocities $(v_{\sigma,K})^{\pm}$ and to bring in an upwind-bias in the mass flux $F_{\sigma,K}$, we define

$$(3.4) \quad (v_{\sigma,K}^n)^+ := u_{\sigma,K}^{n,+} - \delta u_{\sigma,K}(\rho^{n+1})^- \geq 0, \quad (v_{\sigma,K}^n)^- := u_{\sigma,K}^{n,-} - \delta u_{\sigma,K}(\rho^{n+1})^+ \leq 0.$$

We have denoted by $a^{\pm} = \frac{1}{2}(a \pm |a|)$, that splits a real number a in positive and negative valued parts respectively.

- (ii) For a fixed $i = 1, 2, \dots, d$, for each $\sigma \in \mathcal{E}^{(i)}$, $\epsilon \in \tilde{\mathcal{E}}(D_{\sigma})$ and $(\rho, \mathbf{v}, u) \in L_{\mathcal{M}}(\Omega) \times \mathbf{H}_{\mathcal{E},0} \times H_{\mathcal{E},0}^{(i)}$, the net upwind momentum convection flux through the edges of the dual cell D_{σ} is given by the expression

$$(3.5) \quad \sum_{\epsilon \in \tilde{\mathcal{E}}(D_{\sigma})} F_{\epsilon,\sigma}(\rho, \mathbf{v}) u_{\epsilon,\text{up}},$$

where $F_{\epsilon,\sigma}(\rho, \mathbf{v})$ is the mass flux across the edge ϵ of the dual cell D_{σ} . We follow the convention that $F_{\epsilon,\sigma} = 0$ if $\epsilon \in \mathcal{E}_{\text{ext}}$, otherwise it is defined as a suitable linear combination of the primal mass convection fluxes through the neighbouring primal edges with constant coefficients; see [31] for details.

- (iii) The following upwind choice is used for obtaining $u_{\epsilon,\text{up}}$:

$$(3.6) \quad u_{\epsilon,\text{up}} = \begin{cases} u_{\sigma}, & \text{if } F_{\epsilon,\sigma}(\rho, \mathbf{v}) \geq 0, \\ u_{\sigma'}, & \text{otherwise,} \end{cases}$$

where $\epsilon \in \tilde{\mathcal{E}}(D_{\sigma})$, $\epsilon = D_{\sigma}|D_{\sigma'}$.

Definition 3.3 (Discrete gradient and discrete divergence). The discrete gradient operator $\nabla_{\mathcal{E}} : L_{\mathcal{M}}(\Omega) \rightarrow \mathbf{H}_{\mathcal{E},0}(\Omega)$ is defined by the map $q \mapsto \nabla_{\mathcal{E}} q = \left(\partial_{\mathcal{E}}^{(1)} q, \partial_{\mathcal{E}}^{(2)} q, \dots, \partial_{\mathcal{E}}^{(d)} q \right)$, where for each

$i = 1, 2, \dots, d$, $\partial_{\mathcal{E}}^{(i)} q$ denotes

$$(3.7) \quad \partial_{\mathcal{E}}^{(i)} q = \sum_{\sigma \in \mathcal{E}_{\text{int}}^{(i)}} (\partial_{\mathcal{E}}^{(i)} q)_{\sigma} \mathcal{X}_{D_{\sigma}}, \text{ with } (\partial_{\mathcal{E}}^{(i)} q)_{\sigma} = \frac{|\sigma|}{|D_{\sigma}|} (q_L - q_K) \mathbf{e}^{(i)} \cdot \boldsymbol{\nu}_{\sigma, K}, \sigma = K|L \in \mathcal{E}_{\text{int}}^{(i)}.$$

We set the gradient to zero on the external faces. The discrete divergence operator $\text{div}_{\mathcal{M}} : \mathbf{H}_{\mathcal{E},0}(\Omega) \rightarrow L_{\mathcal{M}}(\Omega)$ is defined as $\mathbf{v} \mapsto \text{div}_{\mathcal{M}} \mathbf{v} = \sum_{K \in \mathcal{M}} (\text{div}_{\mathcal{M}} \mathbf{v})_K \mathcal{X}_K$, where for each $K \in \mathcal{M}$, $(\text{div}_{\mathcal{M}} \mathbf{v})_K$ denotes

$$(3.8) \quad (\text{div}_{\mathcal{M}} \mathbf{v})_K = \frac{1}{|K|} \sum_{\sigma \in \mathcal{E}(K)} |\sigma| v_{\sigma, K}.$$

The above discrete operators satisfy the following ‘gradient-divergence duality’; see [31] for further details.

Proposition 3.4. *For any $(q, \mathbf{v}) \in L_{\mathcal{M}}(\Omega) \times \mathbf{H}_{\mathcal{E},0}(\Omega)$, the gradient-divergence duality is given by*

$$(3.9) \quad \int_{\Omega} q (\text{div}_{\mathcal{M}} \mathbf{v}) d\mathbf{x} + \int_{\Omega} \nabla_{\mathcal{E}} q \cdot \mathbf{v} d\mathbf{x} = 0.$$

In the following, we state the so-called ‘inf-sup stability’ satisfied by the MAC grid discretisation introduced above. It is well known from the literature, e.g. [23], that this condition is crucial in establishing the well-posedness of finite element formulations. As mentioned in the introduction, the inf-sup stability is the key to maintaining the stability of the elliptic problem satisfied by the pressure in L^2 -norm. Along the lines of [39], we further deduce that this bound subsequently allows the passage to the incompressible limit of the discrete pressure gradient term. The inf-sup stability can be stated as follows.

Lemma 3.5 (Inf-sup Stability). *There exists a constant $\beta > 0$, depending only on Ω and the discretisation, such that for all $p = \{p_K : K \in \mathcal{M}\}$, there exists $\mathbf{u} = \{u_{\sigma,i} : \sigma \in \mathcal{E}^{(i)}, 1 \leq i \leq d\}$ in $\mathbf{H}_{\mathcal{E},0}$ satisfying*

$$(3.10) \quad \|\mathbf{u}\|_{1,\mathcal{T}} = 1 \text{ and } \sum_{K \in \mathcal{M}} |K| p_K (\text{div } \mathbf{u})_K \geq \beta \|p - m(p)\|_{L^2(\Omega)}.$$

Here, $\|\cdot\|_{1,\mathcal{T}}$ is the discrete H_0^1 norm and $m(p) = \frac{1}{|\Omega|} \int_{\Omega} p d\mathbf{x}$; see, e.g. [25, 28, 55], for more details.

4. AN ENERGY STABLE SEMI-IMPLICIT UPWIND SCHEME

In the following, we introduce our semi-implicit in time, upwind in space, fully-discrete scheme for the Euler system (2.16)-(2.17).

4.1. The scheme. Let us consider a discretisation $0 = t^0 < t^1 < \dots < t^N = T$ of the time-interval $(0, T)$ and let $\delta t = t^{n+1} - t^n$, for $n = 0, 1, \dots, N-1$, be the constant time-step. We consider the following fully-discrete scheme for $0 \leq n \leq N-1$:

$$(4.1) \quad \frac{1}{\delta t} (\rho_K^{n+1} - \rho_K^n) + \frac{1}{|K|} \sum_{\sigma \in \mathcal{E}(K)} F_{\sigma, K}(\rho^{n+1}, \mathbf{v}^n) = 0, \forall K \in \mathcal{M},$$

$$(4.2) \quad \frac{1}{\delta t} (\rho_{D_{\sigma}}^{n+1} u_{\sigma}^{n+1} - \rho_{D_{\sigma}}^n u_{\sigma}^n) + \frac{1}{|D_{\sigma}|} \sum_{\epsilon \in \mathcal{E}(D_{\sigma})} F_{\epsilon, \sigma}(\rho^{n+1}, \mathbf{v}^n) u_{\epsilon, \text{up}}^n + \frac{1}{\epsilon_2} (\partial_{\mathcal{E}}^{(i)} p^{n+1})_{\sigma} = 0, \forall 1 \leq i \leq d, \forall \sigma \in \mathcal{E}_{\text{int}}^{(i)}.$$

The mass balance equation (4.1) is defined on primal mesh cells, whereas the momentum balance (4.2) is on the dual cells. To derive the energy stability, we recall the following mass balance on the dual cell D_σ [31]:

$$(4.3) \quad \frac{1}{\delta t}(\rho_{D_\sigma}^{n+1} - \rho_{D_\sigma}^n) + \frac{1}{|D_\sigma|} \sum_{\epsilon \in \tilde{\mathcal{E}}(D_\sigma)} F_{\epsilon, \sigma}(\rho^{n+1}, \mathbf{v}^n) = 0.$$

The discrete momentum update (4.2) and the dual mass balance (4.3) together yield the following update of the velocity components:

$$(4.4) \quad \frac{u_\sigma^{n+1} - u_\sigma^n}{\delta t} + \frac{1}{|D_\sigma|} \sum_{\epsilon \in \tilde{\mathcal{E}}(D_\sigma)} F_{\epsilon, \sigma}(\rho^{n+1}, \mathbf{v}^n) - \frac{u_\sigma^n - u_\sigma^n}{\rho_{D_\sigma}^{n+1}} + \frac{1}{\varepsilon^2} \frac{(\partial_\mathcal{E}^{(i)} p^{n+1})_\sigma}{\rho_{D_\sigma}^{n+1}} = 0.$$

4.1.1. *Initialisation of the Scheme.* We take initial approximations for ρ and \mathbf{u} as the averages of the initial conditions ρ_0 and \mathbf{u}_0 on primal and dual cells, respectively, to get the initial values:

$$(4.5) \quad \begin{aligned} \rho_K^0 &= \frac{1}{|K|} \int_K \rho_0(\mathbf{x}) d\mathbf{x}, \quad \forall K \in \mathcal{M}, \\ u_{\sigma, i}^0 &= \frac{1}{|D_\sigma|} \int_{D_\sigma} (\mathbf{u}_0(\mathbf{x}))_i d\mathbf{x}, \quad \text{for } 1 \leq i \leq d, \quad \forall \sigma \in \mathcal{E}_{\text{int}}^{(i)}. \end{aligned}$$

In the following lemma, we observe an immediate implication of the ill-prepared initial data from Definition 2.2 in the light of the above discretisation.

Lemma 4.1. *Let the initial condition $(\rho_0^\varepsilon, \mathbf{u}_0^\varepsilon)$ be ill-prepared in the sense of Definition 2.2. Then there exists a constant $C > 0$, independent of ε , such that*

$$(4.6) \quad \frac{1}{\varepsilon} \max_{K \in \mathcal{M}} |(\rho^\varepsilon)_K^0 - 1| \leq C.$$

Proof. For each $K \in \mathcal{M}$ and $\varepsilon > 0$, we have from (4.5) and Definition 2.2 that there exists a constant $C > 0$, independent of ε , such that

$$(4.7) \quad \frac{1}{\varepsilon} |(\rho^\varepsilon)_K^0 - 1| \leq \frac{1}{\varepsilon} \frac{1}{|K|} \int_K |\rho_0^\varepsilon - 1| d\mathbf{x} \leq \frac{1}{\varepsilon} \|\rho_0^\varepsilon - 1\|_{L^\infty(K)} \leq C,$$

which proves the required estimate (4.6). \square

4.2. **Existence of a Numerical Solution.** The mass update (4.1) is nonlinear in ρ^{n+1} due to the presence of the stabilisation terms. However, once ρ^{n+1} is calculated, the momentum update (4.2) can be explicitly evaluated to get the velocity. In what follows, we establish the existence of a discrete solution to the numerical scheme (4.1)-(4.2). Our treatment is analogous to the one in [24, 30, 49, 51] which uses the classical tools from topological degree theory in finite dimensions to hyperbolic problems; see also [17].

Theorem 4.2. *Let $(\rho^n, \mathbf{u}^n) \in L_{\mathcal{M}}(\Omega) \times \mathbf{H}_{\mathcal{E}, 0}(\Omega)$ be such that $\rho^n > 0$ on Ω . Then, there exists a solution $(\rho^{n+1}, \mathbf{u}^{n+1}) \in L_{\mathcal{M}}(\Omega) \times \mathbf{H}_{\mathcal{E}, 0}(\Omega)$ of (4.1)-(4.2), satisfying $\rho^{n+1} > 0$ on Ω .*

Proof. Let $C > 0$ be a constant such that

$$(4.8) \quad C > \frac{|\Omega| \max_{K \in \mathcal{M}} \{\rho_K^n\}}{\min_{K \in \mathcal{M}} \{|K|\}}.$$

Consider the bounded, open subset V of $L_{\mathcal{M}}(\Omega)$ defined by

$$V = \left\{ \rho = \sum_{K \in \mathcal{M}} \rho_K \chi_K \in L_{\mathcal{M}}(\Omega) : 0 < \rho_K < C, \quad \forall K \in \mathcal{M} \right\}.$$

We introduce a continuous function $H : [0, 1] \times L_{\mathcal{M}}(\Omega) \rightarrow L_{\mathcal{M}}(\Omega)$, via $H(\lambda, \rho) = \sum_{K \in \mathcal{M}} H(\lambda, \rho)_K \mathcal{X}_K$, where

$$H(\lambda, \rho)_K = \frac{1}{\delta t}(\rho_K - \rho_K^n) + \frac{\lambda}{|K|} \sum_{\sigma \in \mathcal{E}(K)} F_{\sigma, K}(\rho, \mathbf{v}), \quad \forall K \in \mathcal{M},$$

with $v_\sigma = u_\sigma^n - \frac{\eta \delta t}{\varepsilon^2} (\partial_{\mathcal{E}}^{(i)} p(\rho))_\sigma$. It is easy to note that $H(\lambda, \rho)$ is a homotopy connecting $H(0, \rho)$ and $H(1, \rho)$. In order to establish the existence of a discrete solution $\rho^{n+1} > 0$ of (4.1), we need to show that for any $\lambda \in [0, 1]$, $H(\lambda, \cdot)$ has a non-zero topological degree with respect to V . In other words, we need to show that $H(\lambda, \cdot) \neq 0$ on ∂V , for all $\lambda \in [0, 1]$. On the contrary, let us assume that $H(\lambda, \rho) = 0$, for some $\lambda \in [0, 1]$ and $\rho \in \partial V$, which implies

$$(4.9) \quad \frac{1}{\delta t}(\rho_K - \rho_K^n) + \frac{\lambda}{|K|} \sum_{\sigma \in \mathcal{E}(K)} F_{\sigma, K}(\rho, \mathbf{v}) = 0, \quad \forall K \in \mathcal{M}.$$

Summing (4.9) over all $K \in \mathcal{M}$, and using the definition of C from (4.8), we obtain

$$(4.10) \quad \rho_K \leq \frac{|\Omega| \max_{K \in \mathcal{M}} \{\rho_K^n\}}{\min_{K \in \mathcal{M}} \{|K|\}} < C, \quad \forall K \in \mathcal{M}.$$

Using (4.9), we have for each $K \in \mathcal{M}$ and any $\lambda \in [0, 1]$,

$$(4.11) \quad \rho_K \left[|\Omega| + \lambda \delta t \sum_{\substack{\sigma \in \mathcal{E}(K) \\ \sigma = K|L}} |\sigma| \mathbf{v}_{\sigma, K}^+ \right] > 0.$$

Combining the above inequality with (4.10) gives $0 < \rho_K < C$, for each $K \in \mathcal{M}$, a contradiction as $\rho \in \partial V$. Hence, $0 \notin H(\{\lambda\} \times \partial V)$ for any $\lambda \in [0, 1]$, and by topological degree arguments for finite dimensional spaces [17], we get that $\deg(H(1, \cdot), V, 0) = \deg(H(0, \cdot), V, 0)$. Since $\deg(H(0, \cdot), V, 0) \neq 0$ we further conclude that $H(1, \cdot)$ has a zero in V , i.e. there exists a solution $\rho^{n+1} \in L_{\mathcal{M}}(\Omega)$ of (4.1), such that $\rho^{n+1} > 0$. \square

4.3. Discrete Energy Estimates. This section is devoted to proving apriori energy estimates satisfied by the scheme (4.1)-(4.2) which are discrete counterparts of the stability estimates stated in Proposition 2.4.

Lemma 4.3 (Discrete positive renormalisation identity). *Any solution to the system (4.1)-(4.2) satisfies the following equality:*

$$(4.12) \quad \frac{|K|}{\delta t} [\Pi_\gamma(\rho_K^{n+1}) - \Pi_\gamma(\rho_K^n)] + |K| p_K^{n+1} (\operatorname{div}_{\mathcal{M}} \mathbf{v}^n)_K \\ + \sum_{\substack{\sigma \in \mathcal{E}(K) \\ \sigma = K|L}} |\sigma| \left[(\psi_\gamma(\rho_K^{n+1}) - \rho_K^{n+1} \psi'_\gamma(1)) (v_{\sigma, K}^n)^+ + (\psi_\gamma(\rho_L^{n+1}) - \rho_L^{n+1} \psi'_\gamma(1)) (v_{\sigma, K}^n)^- \right] + R_{K, \delta t}^{n+1} = 0,$$

where the non-negative remainder term is defined by

$$(4.13) \quad R_{K, \delta t}^{n+1} = \frac{|K|}{2\delta t} (\rho_K^{n+1} - \rho_K^n)^2 \psi''_\gamma(\bar{\rho}_K^{n+\frac{1}{2}}) + \sum_{\sigma \in \mathcal{E}(K)} |\sigma| (-(v_{\sigma, K}^n)^-) (\rho_L^{n+1} - \rho_K^{n+1})^2 \psi''_\gamma(\bar{\rho}_\sigma^{n+1}).$$

Proof. The proof follows from the definition of Π_γ and straightforward calculations; see [37, Lemma A.2] for details. \square

Lemma 4.4 (Discrete kinetic energy identity). *Any solution to the system (4.1)-(4.2) satisfies the following equality for $1 \leq i \leq d$, $\sigma \in \mathcal{E}_{\text{int}}^{(i)}$ and $0 \leq n \leq N-1$:*

$$(4.14) \quad \begin{aligned} \frac{1}{2} \frac{|D_\sigma|}{\delta t} (\rho_{D_\sigma}^{n+1} (u_\sigma^{n+1})^2 - \rho_{D_\sigma}^n (u_\sigma^n)^2) + \sum_{\epsilon \in \tilde{\mathcal{E}}(D_\sigma)} F_{\epsilon, \sigma}(\rho^{n+1}, \mathbf{v}^n) \frac{|u_\epsilon^n|^2}{2} + \frac{1}{\varepsilon^2} |D_\sigma| v_\sigma^n (\partial_{\mathcal{E}}^{(i)} p^{n+1})_\sigma + R_{\sigma, \delta t}^{n+1} \\ = -\frac{\eta \delta t}{\varepsilon^4} |D_\sigma| (\partial_{\mathcal{E}}^{(i)} p^{n+1})_\sigma^2, \end{aligned}$$

where the remainder term $R_{\sigma, \delta t}^{n+1}$ is defined by

$$(4.15) \quad R_{\sigma, \delta t}^{n+1} = -\frac{|D_\sigma|}{2\delta t} \rho_{D_\sigma}^{n+1} (u_\sigma^{n+1} - u_\sigma^n)^2 - \sum_{\substack{\epsilon \in \tilde{\mathcal{E}}(D_\sigma) \\ \epsilon = D_\sigma | D_{\sigma'}}} F_{\epsilon, \sigma}(\rho^{n+1}, \mathbf{v}^n) - \frac{(u_\sigma^n - u_{\sigma'}^n)^2}{2}.$$

Proof. Multiplying the momentum balance equation (4.2) by $|D_\sigma| u_\sigma^n$ and using the dual mass balance (4.3) completes the proof. \square

Theorem 4.5 (Total energy balance). *Any solution to the system (4.1)-(4.2) satisfies the following entropy inequality:*

$$(4.16) \quad \frac{1}{\varepsilon^2} \sum_{K \in \mathcal{M}} |K| \Pi_\gamma(\rho_K^{n+1}) + \sum_{\sigma \in \mathcal{E}_{\text{int}}} |D_\sigma| \frac{1}{2} \rho_{D_\sigma}^{n+1} (u_\sigma^{n+1})^2 \leq \frac{1}{\varepsilon^2} \sum_{K \in \mathcal{M}} |K| \Pi_\gamma(\rho_K^n) + \sum_{\sigma \in \mathcal{E}_{\text{int}}} |D_\sigma| \frac{1}{2} \rho_{D_\sigma}^n (u_\sigma^n)^2,$$

under the conditions $\forall \sigma \in \mathcal{E}_{\text{int}}^{(i)}$, $1 \leq i \leq d$:

$$(i) \quad \eta \geq \frac{1}{\rho_{D_\sigma}^{n+1}},$$

$$(ii) \quad \frac{\delta t}{|D_\sigma|} \sum_{\epsilon \in \tilde{\mathcal{E}}(D_\sigma)} \frac{-F_{\epsilon, \sigma}(\rho^{n+1}, \mathbf{v}^n)}{\rho_{D_\sigma}^{n+1}} \leq \frac{1}{2}.$$

Proof. We take the sum over $K \in \mathcal{M}$ in (4.12) and over $\sigma \in \mathcal{E}_{\text{int}}$ in (4.14), and add the resulting equations to get

$$(4.17) \quad \begin{aligned} \frac{1}{\varepsilon^2 \delta t} \sum_{K \in \mathcal{M}} |K| (\Pi_\gamma(\rho_K^{n+1}) - \Pi_\gamma(\rho_K^n)) + \sum_{\sigma \in \mathcal{E}_{\text{int}}} \frac{1}{2} \frac{|D_\sigma|}{\delta t} (\rho_{D_\sigma}^{n+1} (u_\sigma^{n+1})^2 - \rho_{D_\sigma}^n (u_\sigma^n)^2) \\ + \mathcal{R}_{\mathcal{M}, \delta t}^{n+1} + \mathcal{R}_{\mathcal{E}, \delta t}^{n+1} = -\frac{\eta \delta t}{\varepsilon^4} \sum_{i=1}^d \sum_{\sigma \in \mathcal{E}_{\text{int}}^{(i)}} |D_\sigma| (\partial_{\mathcal{E}}^{(i)} p^{n+1})_\sigma^2, \end{aligned}$$

where the global remainder terms $\mathcal{R}_{\mathcal{M}}$ and $\mathcal{R}_{\mathcal{E}}$ are obtained by summing the local remainders R_K and R_σ , respectively. Clearly, $\mathcal{R}_{\mathcal{M}}$ is non-negative unconditionally. In order to derive a condition to make $\mathcal{R}_{\mathcal{E}}$ non-negative, we apply the inequality $(a+b)^2 \leq 2(a^2+b^2)$, $a, b \in \mathbb{R}$ in the velocity update (4.4) and the Cauchy-Schwarz inequality on the second term of $\mathcal{R}_{\mathcal{E}}$ analogously as in [20,

Lemma 3.1] and finally obtain

$$\begin{aligned}
& \frac{1}{\varepsilon^2 \delta t} \sum_{K \in \mathcal{M}} |K| \left(\Pi_\gamma(\rho_K^{n+1}) - \Pi_\gamma(\rho_K^n) \right) + \sum_{\sigma \in \mathcal{E}_{\text{int}}} \frac{1}{2} \frac{|D_\sigma|}{\delta t} \left(\rho_{D_\sigma}^{n+1} (u_\sigma^{n+1})^2 - \rho_{D_\sigma}^n (u_\sigma^n)^2 \right) \\
& + \frac{\delta t}{\varepsilon^4} \sum_{i=1}^d \sum_{\sigma \in \tilde{\mathcal{E}}_{\text{int}}^{(i)}} \left(\eta - \frac{1}{\rho_{D_\sigma}^{n+1}} \right) (\partial_{\mathcal{E}}^{(i)} p^{n+1})_\sigma^2 \\
(4.18) \quad & \leq \sum_{\sigma \in \mathcal{E}_{\text{int}}} \left(\frac{1}{2} - \frac{\delta t}{|D_\sigma|} \sum_{\epsilon \in \mathcal{E}(D_\sigma)} \frac{-(F_{\epsilon, \sigma}(\rho^{n+1}, \mathbf{v}^n))^-}{\rho_{D_\sigma}^{n+1}} \right) \left(\sum_{\substack{\epsilon \in \tilde{\mathcal{E}}(D_\sigma) \\ \epsilon = D_\sigma | D_{\sigma'} }} F_{\epsilon, \sigma}(\rho^{n+1}, \mathbf{v}^n)^- (u_\sigma^n - u_{\sigma'}^n)^2 \right).
\end{aligned}$$

Note that the right hand side is non-positive under the time step restriction

$$\frac{\delta t}{|D_\sigma|} \sum_{\epsilon \in \tilde{\mathcal{E}}(D_\sigma)} \frac{-F_{\epsilon, \sigma}(\rho^{n+1}, \mathbf{v}^n)^-}{\rho_{D_\sigma}^{n+1}} \leq \frac{1}{2},$$

and the third term on the left hand side is non-negative under the condition $\eta \geq \frac{1}{\rho_{D_\sigma}^{n+1}}$. \square

Remark 4.6. The conditions (i) and (ii) in the above theorem are implicit in nature. However, we observe that the following implicit time-step restriction

$$(4.19) \quad \frac{\delta t}{|D_\sigma|} \sum_{\epsilon \in \tilde{\mathcal{E}}(D_\sigma)} \frac{|F_{\epsilon, \sigma}(\rho^{n+1}, \mathbf{v}^n)|}{\rho_{D_\sigma}^{n+1}} \leq \frac{1}{2}$$

gives a sufficient condition from which we can deduce the condition (ii). Now, from (4.19) and the dual mass balance (4.3), we have

$$(4.20) \quad \frac{3}{2} \rho_{D_\sigma}^{n+1} - \rho_{D_\sigma}^n \geq \rho_{D_\sigma}^{n+1} - \rho_{D_\sigma}^n + \frac{\delta t}{|D_\sigma|} \sum_{\epsilon \in \tilde{\mathcal{E}}(D_\sigma)} |F_{\epsilon, \sigma}(\rho^{n+1}, \mathbf{v}^n)| \geq 0.$$

Hence, we get

$$(4.21) \quad \frac{\rho_{D_\sigma}^n}{\rho_{D_\sigma}^{n+1}} \leq \frac{3}{2}.$$

Therefore, at each interface σ , choosing η such that $\eta = \eta_1 / \rho_{D_\sigma}^n$ with $\eta_1 > \frac{3}{2}$ will guarantee the condition (i) and hence the stability of the scheme. In other words, the value of η can be obtained explicitly. Analogous considerations can also be found in [21].

5. WEAK CONSISTENCY OF THE SCHEME

Goal of this section is to show a Lax-Wendroff-type weak consistency of the scheme (4.1)-(4.2) which is essentially proving the consistency of the numerical solution with a weak solution of the Euler system when the mesh parameters tend to zero. To this end, we have borrowed the tools developed in [26, 27] to prove weak consistency of finite volume discretisations of general convective operators.

Definition 5.1. $(\rho^\varepsilon, \mathbf{u}^\varepsilon) \in L^\infty(Q)^{1+d}$ is a weak solution to the Euler system (2.1)-(2.2) with initial-boundary conditions (2.3) if $\rho^\varepsilon > 0$ a.e. in Q and the following identities hold:

$$(5.1) \quad \int_0^T \int_\Omega (\rho^\varepsilon \partial_t \psi + \rho^\varepsilon \mathbf{u}^\varepsilon \cdot \nabla_x \psi) \, d\mathbf{x} dt = - \int_\Omega \rho_0^\varepsilon \psi(0, \cdot) \, d\mathbf{x}, \text{ for all } \psi \in C_c^\infty([0, T] \times \bar{\Omega}),$$

$$(5.2) \quad \int_0^T \int_\Omega (\rho^\varepsilon \mathbf{u}^\varepsilon \cdot \partial_t \psi + (\rho^\varepsilon \mathbf{u}^\varepsilon \otimes \mathbf{u}^\varepsilon) : \nabla_x \psi) \, d\mathbf{x} dt + \int_0^T \int_\Omega p^\varepsilon \nabla_x \psi \, d\mathbf{x} dt = - \int_\Omega \rho_0^\varepsilon \mathbf{u}_0^\varepsilon \cdot \psi(0, \cdot) \, d\mathbf{x},$$

for all $\psi \in C_c^\infty([0, T] \times \bar{\Omega})^d$.

The following theorem is a Lax-Wendroff-type consistency formulation for the semi-implicit scheme (4.1)-(4.2).

Theorem 5.2. Let Ω be an open bounded subset of \mathbb{R}^d . Assume that $(\mathcal{T}^{(m)}, \delta t^{(m)})_{m \in \mathbb{N}}$ is a sequence of discretisations such that both $\lim_{m \rightarrow +\infty} \delta t^{(m)}$ and $\lim_{m \rightarrow +\infty} h^{(m)}$ are 0. Let $(\rho^{(m)}, \mathbf{u}^{(m)})_{m \in \mathbb{N}}$ be the corresponding sequence of discrete solutions with respect to an initial data $(\rho_0^\varepsilon, \mathbf{u}_0^\varepsilon) \in L^\infty(\Omega)^{1+d}$. We assume that $(\rho^{(m)}, \mathbf{u}^{(m)})_{m \in \mathbb{N}}$ satisfies the following:

$(\rho^{(m)}, \mathbf{u}^{(m)})_{m \in \mathbb{N}}$ is uniformly bounded in $L^\infty(Q)^{1+d}$, i.e.

$$(5.3) \quad \underline{C} \leq (\rho^{(m)})_K^n \leq \bar{C}, \quad \forall K \in \mathcal{M}^{(m)}, \quad 0 \leq n \leq N^{(m)}, \quad \forall m \in \mathbb{N},$$

$$(5.4) \quad |(u^{(m)})_\sigma^n| \leq C, \quad \forall \sigma \in \mathcal{E}^{(m)}, \quad 0 \leq n \leq N^{(m)}, \quad \forall m \in \mathbb{N}.$$

where \underline{C}, \bar{C} and C are positive constants independent of the discretisations. We also assume that there exists $\theta > 0$ such that the sequence of discretisations $(\mathcal{T}^{(m)}, \delta t^{(m)})_{m \in \mathbb{N}}$ satisfies the condition:

$$(5.5) \quad \frac{\delta t^{(m)}}{\min_{K \in \mathcal{M}^{(m)}} |K|} \leq \theta, \quad \max_{K \in \mathcal{M}^{(m)}} \frac{\text{diam}(K)^2}{|K|} \leq \theta, \quad \forall m \in \mathbb{N}.$$

We suppose that the sequence $(\rho^{(m)}, \mathbf{u}^{(m)})_{m \in \mathbb{N}}$ converges to $(\rho_\varepsilon, \mathbf{u}_\varepsilon) \in L^\infty(Q)^{1+d}$ as $m \rightarrow \infty$ in $L^r(Q)^{1+d}$ for $1 \leq r < \infty$. Then $(\rho_\varepsilon, \mathbf{u}_\varepsilon)$ satisfies the weak formulation (5.1)-(5.2).

Proof. Our approach follows analogous lines as in [27, Lemma 4.1] and hence we skip most of the calculations except the ones related to the velocity stabilisation term. Proceeding as in [27, Lemma 4.1], the additional term $R^{(m)}$ arising from the mass update (4.1) can be obtained as

$$(5.6) \quad R^{(m)} = C_\psi \sum_{n=0}^{N^{(m)}-1} \delta t^n \sum_{K \in \mathcal{M}} \text{diam}(K) \sum_{\sigma \in \mathcal{E}(K)} |\sigma| |\delta u_\sigma(\rho^{n+1})|,$$

where C_ψ is a constant depending only on the test function $\psi \in C_c^\infty([0, T] \times \bar{\Omega})$. Using (5.3), $R^{(m)}$ can be further estimated as

$$(5.7) \quad R^{(m)} \leq \gamma \bar{C}^{\gamma-1} C_\psi \sum_{n=0}^{N^{(m)}-1} \delta t^n \sum_{K \in \mathcal{M}} \text{diam}(K) \sum_{\sigma \in \mathcal{E}(K)} |\sigma| \eta \delta t^n \frac{|\sigma|}{|D_\sigma|} |\rho_L^{n+1} - \rho_K^{n+1}|.$$

Using the tools introduced in [26, Section 4] to study the convergence of discrete space translates, it can be shown that the right hand side of (5.7) tends to 0 as $m \rightarrow \infty$ under the assumptions (5.3) and (5.5); see also [27, Lemma A.1] for a similar treatment on discrete space translates. The consistency of the discrete convection operator and the pressure gradient in the momentum update (4.2) can be obtained under the given assumptions using a similar method as in the proof of [38, Theorem 4.1]. The residual term appearing due to the velocity stabilisation in the momentum update again converges to 0 by a similar argument used in the case of the mass update. \square

Adopting similar techniques as in the proof of [38, Theorem 5.1] yields the following LW weak-entropy consistency of the velocity stabilised scheme:

Theorem 5.3. *Suppose that all the assumptions (5.3)-(5.5) hold true for the sequence of discrete solutions $(\rho^{(m)}, \mathbf{u}^{(m)})_{m \in \mathbb{N}}$ which converge to $(\rho^\varepsilon, \mathbf{u}^\varepsilon) \in L^\infty(Q)^{1+d}$ in $L^r(Q)^{1+d}$ for $1 \leq r < \infty$. In addition, assume the following discrete BV estimates:*

$$(5.8) \quad \sum_{n=0}^{N^{(m)}-1} \sum_{K \in \mathcal{M}^{(m)}} |K| |(\rho^{(m)})_K^{n+1} - (\rho^{(m)})_K^n| \leq C, \quad \forall m \in \mathbb{N},$$

$$(5.9) \quad \sum_{n=0}^{N^{(m)}-1} \sum_{\sigma \in \mathcal{E}^{(m)}} |D_\sigma| |(u^{(m)})_\sigma^{n+1} - (u^{(m)})_\sigma^n| \leq C, \quad \forall m \in \mathbb{N}$$

where C is a positive constant independent of the mesh parameters. Also assume that the space and time discretisations satisfy the following:

$$(5.10) \quad \lim_{m \rightarrow \infty} \frac{\delta t^{(m)}}{\min_{\sigma \in \mathcal{E}^{(m)}} |\sigma|} = 0.$$

Then, the limiting terms $(\rho^\varepsilon, \mathbf{u}^\varepsilon) \in L^\infty(Q)^{1+d}$ satisfy the entropy condition:

$$(5.11) \quad - \int_0^T \int_\Omega \left[\zeta^\varepsilon \partial_t \psi + \left(\zeta^\varepsilon + \frac{1}{\varepsilon^2} p^\varepsilon \right) \mathbf{u}^\varepsilon \cdot \nabla \psi \right] d\mathbf{x} dt \leq \int_\Omega \zeta_0^\varepsilon \psi(0, x) d\mathbf{x}, \quad \forall \psi \in C_c^\infty([0, T] \times \bar{\Omega}), \quad \psi(T) = 0, \quad \psi \geq 0,$$

where $\zeta^\varepsilon = \frac{1}{\varepsilon^2} \Pi_\gamma(\rho^\varepsilon) + \frac{1}{2} \rho^\varepsilon |\mathbf{u}^\varepsilon|^2$ and $\zeta_0^\varepsilon = \frac{1}{\varepsilon^2} \Pi_\gamma(\rho_0^\varepsilon) + \frac{1}{2} \rho_0^\varepsilon |\mathbf{u}_0^\varepsilon|^2$.

6. CONSISTENCY OF THE SCHEME WITH THE ZERO MACH NUMBER LIMIT

In the present section, we derive the zero Mach number limit of the semi-implicit scheme (4.1)-(4.2) as done in the continuous case in Section 2. We show that the $\varepsilon \rightarrow 0$ limit of the scheme (4.1)-(4.2) is a semi-implicit scheme for the velocity stabilised incompressible Euler system (2.23)-(2.24). In order to establish this asymptotic consistency result, we use the discrete energy estimates obtained from (4.16) and prove the convergence of the numerical solution in the discrete function spaces. We start by proving the following Lemma which gives the entropy inequality for the scheme (4.1)-(4.2).

Lemma 6.1. *Suppose that the initial data $(\rho_0^\varepsilon, \mathbf{u}_0^\varepsilon)$ satisfy the ill-prepared condition (2.2). Then, there exists a constant $C > 0$, independent of ε , such that the numerical solution $(\rho^n, \mathbf{u}^n)_{0 \leq n \leq N}$ satisfies the entropy inequality:*

$$(6.1) \quad \frac{1}{2} \sum_{\sigma \in \mathcal{E}_{\text{int}}} |D_\sigma| |\rho_{D_\sigma}^n| |\mathbf{u}_\sigma^n|^2 + \frac{1}{\varepsilon^2} \sum_{K \in \mathcal{M}} |K| |\Pi_\gamma(\rho_K^n) + \frac{(\delta t)^2}{\varepsilon^4} \sum_{k=0}^{n-1} \sum_{\sigma \in \mathcal{E}_{\text{int}}} \left(\eta - \frac{1}{\rho_{D_\sigma}^{k+1}} \right) |(\nabla_\varepsilon p^{k+1})_\sigma|^2 \leq C.$$

Proof. First, we multiply the total energy balance (4.18) by δt and sum over times k from 0 to $n-1$. Using the estimate (4.6) coming from the ill-prepared data (2.2) and the bounds on Π_γ [39, Lemma 2.3] we can obtain the required result. \square

In the following, we establish claims similar to the ones in [39, Proposition 2.6] for the discrete solution.

Lemma 6.2. *Let $\mathcal{T} = (\mathcal{M}, \mathcal{E})$ be a fixed primal-dual mesh pair that gives a MAC discretisation of $\bar{\Omega}$ and let $\delta t > 0$ be such that $\{0 = t^0 < t^1 < \dots < t^N = T\}$ is a discretisation of the time domain $[0, T]$ with $t^n = n\delta t$, for $1 \leq n \leq N = \lfloor \frac{T}{\delta t} \rfloor$. For each $\varepsilon > 0$, let us denote by*

$(\rho^\varepsilon, \mathbf{u}^\varepsilon) \in L^\infty(0, T; L_{\mathcal{M}}(\Omega) \times \mathbf{H}_{\varepsilon, 0}(\Omega))$, the discrete solution to the semi-implicit scheme (4.1)-(4.2) with respect to the ill-prepared initial data discretised via (4.5). Then, the following holds.

(i) For $\gamma \geq 2$, we have for all $\varepsilon > 0$ sufficiently small

$$(6.2) \quad \frac{1}{\varepsilon} \|\rho^\varepsilon - 1\|_{L^\infty(0, T; L^2(\Omega))} \leq C(\gamma).$$

Also for $\gamma \in (1, 2)$, we have for all $\varepsilon > 0$ sufficiently small, and for any $R \in (2, +\infty)$

$$(6.3) \quad \frac{1}{\varepsilon} \|(\rho^\varepsilon - 1)\mathcal{X}_{\{\rho^\varepsilon < R\}}\|_{L^\infty(0, T; L^2(\Omega))} \leq C(\gamma, R),$$

$$(6.4) \quad \varepsilon^{-\frac{2}{\gamma}} \|(\rho^\varepsilon - 1)\mathcal{X}_{\{\rho^\varepsilon \geq R\}}\|_{L^\infty(0, T; L^\gamma(\Omega))} \leq C(\gamma, R).$$

Here $C(\gamma)$ and $C(\gamma, R)$ are positive constants independent of ε .

(ii) $\rho^\varepsilon \rightarrow 1$ as $\varepsilon \rightarrow 0$ in $L^\infty(0, T; L^r(\Omega))$ for any $r \in (1, \min\{2, \gamma\}]$. Moreover, for any $\gamma > 1$ $\rho^\varepsilon \rightarrow 1$ as $\varepsilon \rightarrow 0$ in $L^\infty(0, T; L^\gamma(\Omega))$.

(iii) The sequence of approximate solutions for the velocity component $(\mathbf{u}^\varepsilon)_{\varepsilon > 0}$ is uniformly bounded with respect to ε , i.e. for all $\varepsilon > 0$ sufficiently small we have

$$(6.5) \quad \|\mathbf{u}^\varepsilon\|_{L^\infty(0, T; L^2(\Omega)^d)} \leq C,$$

where $C > 0$ is a constant independent of ε .

Proof. The estimates for the point-values of the weak solutions derived in [39, Lemma 2.3] make use of the bounds on the relative entropy functional Π_γ which leads to the convergence results [39, Proposition 2.6]. In an analogous manner, we can adopt the same results for the discrete solutions of the present scheme and use the estimate (6.1) to obtain the above convergence results for ρ^ε . Next, we proceed to derive the estimate (6.5) on the velocity. To this end, we first note that for each $n \in \{1, \dots, N\}$, and for each $K \in \mathcal{M}$, we have $\rho_K^n \rightarrow 1$ as $\varepsilon \rightarrow 0$. Since there exists $0 < \rho_{\min} < 1$, we can further conclude that for all $\varepsilon > 0$ sufficiently small,

$$(6.6) \quad \rho_K^n > \rho_{\min}, \quad \forall n \in \{0, \dots, N\}, \quad \forall K \in \mathcal{M}.$$

From the discrete entropy estimate (6.1), the bounds on Π_γ [39, Lemma 2.3] and the estimate (4.6) on ill-prepared initial data we get

$$(6.7) \quad \sum_{i=1}^d \sum_{\sigma \in \mathcal{E}_{\text{int}}^{(i)}} \rho_{D_\sigma}^{n+1} |u_\sigma^{n+1}|^2 \leq C, \quad \forall n \in \{0, \dots, N-1\}.$$

From (6.6) and (6.7) we subsequently obtain the required estimate (6.5). \square

It is well known that an asymptotic analysis of the Euler equations reveals a pressure decomposition $p = p_{(0)} + \varepsilon^2 \pi$ in the low Mach number regime, where the second order pressure π survives as the incompressible pressure in the limit $\varepsilon \rightarrow 0$. In the discrete counterpart, in order that a scheme to be consistent with the incompressible limit, it is therefore essential for the numerical pressure to have the same decomposition and its second order to survive in the limit $\varepsilon \rightarrow 0$. In the following lemma, we give an estimate on the second order pressure, using the uniform boundedness of the pressure gradient $\nabla \mathcal{E} p^n$ appearing in the discrete entropy estimate (6.1). The following estimate is a consequence of the inf-sup stability of the MAC discretisation, cf. Lemma 3.5.

Lemma 6.3 (Bound on the second order pressure). *Let $\varepsilon > 0$ and $(\rho^n, \mathbf{u}^n)_{0 \leq n \leq N}$ be the solution to the scheme (4.1)-(4.2). Define $\pi^n = \sum_{K \in \mathcal{M}} \pi_K^n \mathcal{X}_K$, where $\pi_K^n = \frac{p_K^n - m(\bar{p}^n)}{\varepsilon^2}$ with $m(\bar{p}^n)$ being*

the mean value of p^n over Ω . Then, there exists a constant $C_{\mathcal{T},\delta t}$, independent of ε , such that for $0 \leq n \leq N$

$$(6.8) \quad \|\pi^n\| \leq C_{\mathcal{T},\delta t},$$

where $\|\cdot\|$ is any norm on the discrete function space.

Proof. For a proof we refer to [39, Lemma 7.9], wherein the estimate is obtained for a staggered discretisation. Using the uniform boundedness of the discrete pressure gradient obtained from the estimate (6.1), a similar procedure can be adapted for the MAC discretisation to yield (6.8). \square

As a consequence of the convergence $\rho^\varepsilon \rightarrow 1$, the uniform bounds obtained in Lemma 6.2, and the bound on the second order pressure obtained in Lemma 6.3, we deduce the following theorem which gives a semi-implicit scheme for the incompressible Euler system with velocity stabilisation as the limit of the semi-implicit scheme (4.1)-(4.2) when $\varepsilon \rightarrow 0$.

Theorem 6.4. *Let $(\varepsilon^{(k)})_{k \in \mathbb{N}}$ be a sequence of positive numbers converging to zero, $(\rho^{(k)}, \mathbf{u}^{(k)})_{k \in \mathbb{N}}$ be the corresponding sequence of numerical solutions obtained from the scheme (4.1)-(4.2), and let the initial data $(\rho_0^{(k)}, \mathbf{u}_0^{(k)})$ satisfy (2.2). Then $(\rho^{(k)})_{k \in \mathbb{N}}$ converges to 1 in $L^\infty(0, T; L^\gamma(\Omega))$ and $(\mathbf{u}^{(k)}, \pi^{(k)})_{k \in \mathbb{N}}$ converges to $(\mathbf{u}, \pi) \in L^\infty(0, T; \mathbf{H}_{\mathcal{E},0}(\Omega) \times L_{\mathcal{M}}(\Omega))$ in any discrete norm when k tends to ∞ , where the sequence (\mathbf{u}^n, π^n) is defined as follows. Given $(\mathbf{u}^n, \pi^n) \in \mathbf{H}_{\mathcal{E},0}(\Omega) \times L_{\mathcal{M}}(\Omega)$ at time t^n , $(\mathbf{u}^{n+1}, \pi^{n+1}) \in \mathbf{H}_{\mathcal{E},0}(\Omega) \times L_{\mathcal{M}}(\Omega)$ is obtained as the solution of the following semi-implicit scheme:*

$$(6.9) \quad (\operatorname{div}_{\mathcal{M}}(\mathbf{u}^n - \delta \mathbf{u}(\pi^{n+1})))_K = 0, \quad \forall K \in \mathcal{M},$$

$$(6.10) \quad \frac{1}{\delta t} (u_\sigma^{n+1} - u_\sigma^n) + \frac{1}{|D_\sigma|} \sum_{\epsilon \in \tilde{\mathcal{E}}(D_\sigma)} F_{\epsilon,\sigma}(1, \mathbf{u}^n - \delta \mathbf{u}(\pi^{n+1})) u_{\epsilon,\text{up}}^n + (\partial_{\mathcal{E}}^{(i)} \pi^{n+1})_\sigma = 0, \quad 1 \leq i \leq d, \quad \forall \sigma \in \mathcal{E}_{\text{int}}^{(i)},$$

where the correction $(\delta \mathbf{u}(\pi^{n+1}))_\sigma = \eta \delta t (\partial_{\mathcal{E}}^{(i)} \pi^{n+1})_\sigma$ for $\sigma \in \mathcal{E}_{\text{int}}^{(i)}$, $i = 1, 2, \dots, d$.

Proof. Using the second term on the left hand side of (6.1) we can easily show that $\rho^{(k)} \rightarrow 1$ as $k \rightarrow \infty$ using estimates on Π_γ from Lemma 6.2; see also [39]. From the first term in (6.1) we get the estimate $\|\mathbf{u}^{(k)}\|_{L^2(\Omega)^d} \leq \sqrt{\frac{2C}{\rho_{\min}}}$ for all $k \in \mathbb{N}$. Noting that $\pi^{(k)}$ bounded, cf. (6.8), we conclude that $\|\frac{1}{(\varepsilon^{(k)})^2} \nabla \mathcal{E} p^{(k)}\|$ is bounded and therefore admits a weak limit. Hence, there exists a subsequence of $(\mathbf{u}^{(k)}, \pi^{(k)})_{k \in \mathbb{N}}$ which tends, in any discrete norm, to a limit (\mathbf{u}, π) which satisfies (6.9)-(6.10). \square

7. NUMERICAL RESULTS

In this section, we report the results of extensive numerical tests performed with the semi-implicit scheme (4.1)-(4.2). Note that the stability analysis performed in Section 4, cf. Theorem 4.5, requires that the timesteps δt be chosen according to the condition:

$$(7.1) \quad \frac{\delta t}{|D_\sigma|} \sum_{\epsilon \in \tilde{\mathcal{E}}(D_\sigma)} \frac{-(F_{\epsilon,\sigma}(\rho^{n+1}, \mathbf{v}^n))^-}{\rho_{D_\sigma}^{n+1}} \leq \frac{1}{2}, \quad \forall \sigma \in \mathcal{E}^{(i)}, \quad i = 1, \dots, d.$$

Since the above stability condition is implicit and difficult to carry out, along the lines of [15, 20, 21], we derive a sufficient condition which is easy to implement in practice.

Proposition 7.1. *Suppose $\delta t > 0$ be such that for each $\sigma \in \mathcal{E}^{(i)}$, $i \in \{1, \dots, d\}$, $\sigma = K|L$, the following holds:*

$$(7.2) \quad \delta t \max \left\{ \frac{|\partial K|}{|K|}, \frac{|\partial L|}{|L|} \right\} \left(|u_\sigma^n| + \sqrt{\frac{\eta}{\varepsilon^2} |p_L^{n+1} - p_K^{n+1}|} \right) \leq \min \left\{ 1, \frac{1}{3} \mu_{K,L}^{n,n+1} \right\},$$

where $|\partial K| = \sum_{\sigma \in \mathcal{E}(K)} |\sigma|$ and $\mu_{K,L}^{n,n+1} = \frac{\min\{\rho_K^n, \rho_L^n\}}{\max\{\rho_K^{n+1}, \rho_L^{n+1}\}}$. Then δt satisfies the inequality (7.1).

Proof. The proof follows the same lines of [15, Proposition 3.2], where a similar result has been obtained for an explicit scheme; see also [20, 21] for analogous treatments. \square

In all the numerical case studies performed below, the above condition (7.2) is implemented using the solution at t^n in an explicit manner as in [52]. The time-step restriction (7.2) gives a much less restrictive CFL condition compared to the classical explicit one, e.g. in 1D:

$$(7.3) \quad \text{CFL} = \max \left(|u^n| + \frac{c^n}{\varepsilon} \right) \frac{\delta t}{|K|},$$

where $c^n = \sqrt{\gamma p^n / \rho^n}$. In view of the boundedness of the second order pressure π , cf. Lemma 6.3, we note that δt permitted by (7.2) is $\mathcal{O}(1)$, whereas the classical explicit time-step is $\mathcal{O}(\varepsilon)$ as $\varepsilon \rightarrow 0$. Hence, the semi-implicit scheme (4.1)-(4.2) admits large time-steps at low Mach numbers. In addition, the time-steps remain bounded as $\varepsilon \rightarrow 0$ which is crucial for the AP property of the scheme. The gain in CFL condition in low Mach number computations is recorded in Subsection 7.1.

The numerical implementation of the scheme (4.1)-(4.2) is done as follows. First, the mass conservation equation (4.1) is solved to get the updated density ρ^{n+1} . A Newton iteration has to be performed due to the presence of nonlinear stabilisation terms. In our experiments, we note that iterations converge in 2-3 steps. Once ρ^{n+1} is calculated, the momentum update (4.2) is evaluated explicitly to get the velocity \mathbf{u}^{n+1} .

7.1. 1D Riemann Problems. We consider the following initial data from [16] which consists of several Riemann problems:

$$\begin{aligned} \rho(0, x) &= 1, & q(0, x) &= 1 - \frac{\varepsilon^2}{2}, & x &\in [0, 0.2] \cup [0.8, 1], \\ \rho(0, x) &= 1 + \varepsilon^2, & q(0, x) &= 1, & x &\in (0.2, 0.3], \\ \rho(0, x) &= 1, & q(0, x) &= 1 + \frac{\varepsilon^2}{2}, & x &\in (0.3, 0.7], \\ \rho(0, x) &= 1 - \varepsilon^2, & q(0, x) &= 1, & x &\in (0.7, 0.8], \end{aligned}$$

where $q = \rho u$ denotes the momentum. The pressure law is specified as $p(\rho) = \rho^2$. The computational domain $[0, 1]$ is divided into 200 mesh points and we apply periodic boundary conditions. Computations are carried out up to a time $T = 0.05$ and the time-steps are calculated using (7.2). We set $\varepsilon = 0.8, 0.3, 0.05$ and 0.001 which correspond to the transition from compressible to weakly compressible to almost incompressible regime. The minimum value of the stabilisation parameter η is observed to be 1.5 whereas the maximum value is 4.36 throughout the case studies corresponding to different ε . In Figure 1, we plot the density and momentum profiles against a reference solution obtained using an explicit Rusanov scheme on a mesh resolution of $\Delta x = 1/500$ and $\Delta t = 1/20000$ when $\varepsilon = 0.8, 0.3, 0.05$ and using the classical explicit time-step with $\text{CFL} = 0.9$ as described in (7.3) when $\varepsilon = 0.001$. The figure shows that there are shocks and expansions in the compressible case ($\varepsilon = 0.8$) and as $\varepsilon \rightarrow 0$, the discontinuities get weaker and the flow tends to be smooth. We further observe that both the density and momentum converge to constant values in the almost

incompressible regime $\varepsilon = 10^{-3}$. Hence, the proposed scheme can perform across the three different regimes and can resolve the respective flow features accurately. Furthermore, we note that the maximum value $\max_{i,n} |u_i^n| \Delta t^n / \Delta x$ of the advective Courant number for the present scheme corresponding to $\varepsilon = 0.001$ is 224.64 whereas for the explicit Rusanov scheme it is 0.71. The minimum and maximum values of η computed for this test problem are 1.5 and 4.35 respectively.

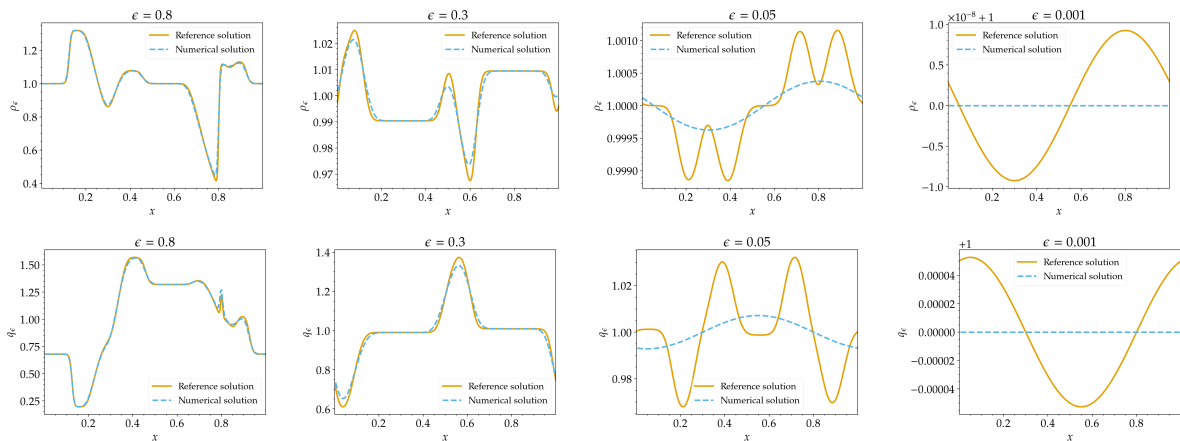


FIGURE 1. Density and momentum plots on top and bottom panels respectively for the 1D Riemann problem at time $T = 0.05$ for $\varepsilon = 0.8, 0.3, 0.05, 0.001$.

In order to demonstrate the positivity preserving property of the scheme, we perform the simulation of the following extreme Riemann problem motivated by the initial data given in [58]:

$$(\rho, u) = \begin{cases} (1, -3) & \text{if } x < 0, \\ (1, 3) & \text{if } x > 0. \end{cases}$$

The computational domain $[-1, 1]$ is divided into 100 mesh points and the final time is $T = 0.15$. The gas constant is $\gamma = 2$, the boundaries are periodic and we set $\varepsilon = 1$ in order to simulate the compressible regime. The density and momentum obtained are given in Figure 2 which clearly indicates the positivity preserving property.

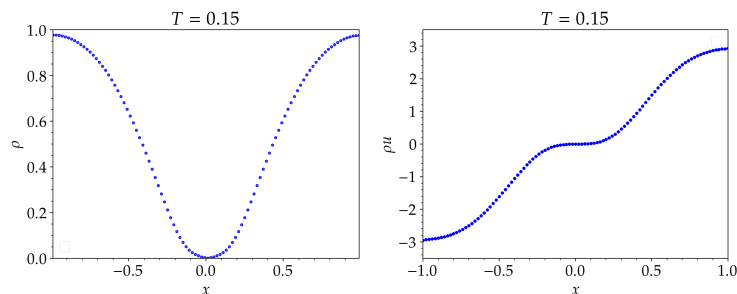


FIGURE 2. Extreme Riemann problem. Plots of the density and momentum at time $T = 0.15$.

7.2. Two Colliding Acoustic Pulses. Here we consider the two colliding acoustic pulses problem from [44], adapted to isentropic flows as done in [16]. The problem describes the advection of large amplitude, short wavelength density perturbations in a weakly compressible flow. The pressure law is taken to be $p(\rho) = \rho^{1.4}$ and the initial density and momentum read

$$\begin{aligned}\rho(0, x) &= 0.955 + \frac{\varepsilon}{2}(1 - \cos(2\pi x)), \\ q(0, x) &= -\text{sign}(x)\sqrt{1.4}(1 - \cos(2\pi x)).\end{aligned}$$

We take the computational domain $[-1, 1]$ which is divided into 100 mesh points. The boundaries are periodic at both the ends. We first plot the initial density profile corresponding to $\varepsilon = 0.1$ using 1000 mesh points in Figure 3. Subsequently, we plot the densities computed at times $T = 0.01, 0.02, 0.04, 0.06, 0.08$ against a reference solution obtained using an explicit Runge-Kutta scheme with a mesh resolution $\Delta x = 1/1000$ and Δt computed using the acoustic time step (7.3) with CFL number 0.5. Analogously, in Figure 4 we plot the momentum profiles at times $T = 0, 0.01, 0.02, 0.04, 0.06, 0.08$. We note the pulses superimpose, separate and this process repeats due to the periodic boundary conditions applied. It can be seen from the densities at $T = 0$ and $T = 0.08$ that because of weakly nonlinear effects, the pulses start to steepen, resulting in the formation of two weak shocks. Furthermore, we observe that the scheme is able to maintain the amplitude of the pulses despite the flow being at low Mach numbers and the initial data being ill-prepared. The minimum and maximum values of η computed for this particular test problem are 1.57 and 1.72, respectively.

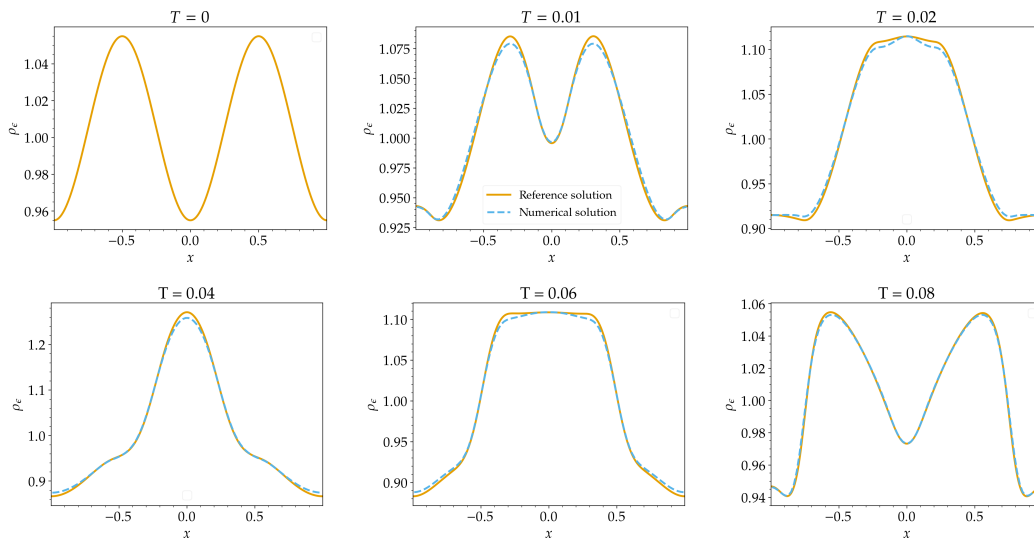


FIGURE 3. Density profiles for the two colliding acoustic pulses problem for $\varepsilon = 0.1$ at times $T = 0, 0.01, 0.02, 0.04, 0.06, 0.08$.

To further demonstrate the scheme's capability to resolve low Mach number flows with ill-prepared initial data, we compute the density and momenta at times $T = 0.001, 0.005, 0.008$ for an even smaller value $\varepsilon = 0.01$. The results are displayed in Figure 5 where the pulses superimpose, gain maximum amplitude and separate.

7.3. Advecting Vortex. Drawing inspiration from [3], we consider the following advecting vortex problem which is a case study used to analyse the numerical dissipation of explicit time-stepping

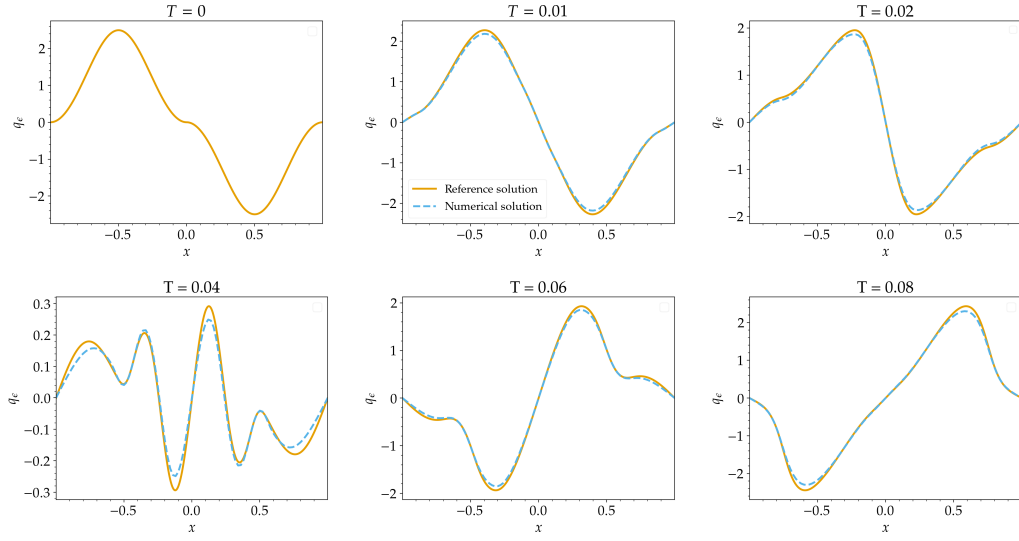


FIGURE 4. Momentum profiles for the two colliding acoustic pulses problem for $\varepsilon = 0.1$ at times $T = 0, 0.01, 0.02, 0.04, 0.06, 0.08$.

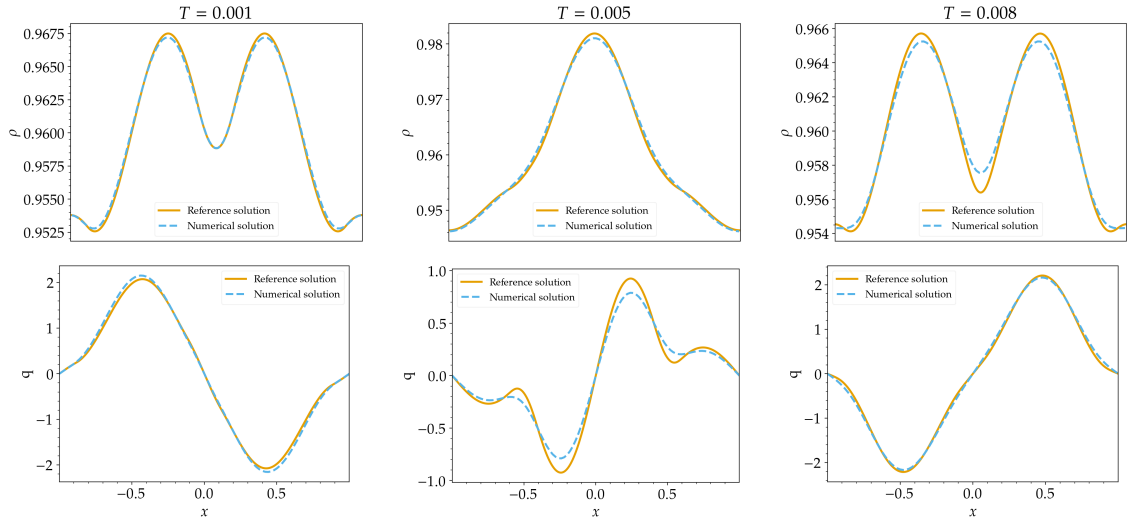


FIGURE 5. Density and momentum profiles for the two colliding acoustic pulses problem for $\varepsilon = 0.01$ at times $T = 0.001, 0.005, 0.008$.

schemes. It has been reported in the literature that the dissipation increases with decreasing Mach numbers. The moving vortex is a low Mach number flow which does not contain acoustic waves. A radially symmetric vortex is placed at the point $(x_0, y_0) = (0.5, 0.5)$ in the computational domain

$\Omega = [0, 1] \times [0, 1]$. The initial data read

$$\begin{aligned}\rho(0, x, y) &= 110 + \left(\frac{\zeta\Gamma}{\omega}\right)^2 (k(\omega r) - k(\pi))\mathcal{X}_{\omega r \leq \pi}, \\ u(0, x, y) &= 0.1 + \Gamma(1 + \cos(\omega r))(0.5 - y)\mathcal{X}_{\omega r \leq \pi}, \\ v(0, x, y) &= \Gamma(1 + \cos(\omega r))(0.5 - x)\mathcal{X}_{\omega r \leq \pi},\end{aligned}$$

where $r = \sqrt{(x - x_0)^2 + (y - y_0)^2}$. We set $\Gamma = 1.5$, $\omega = 4\pi$ and $k(r) = 2\cos(r) + 2r\sin(r) + \frac{1}{8}\cos(2r) + \frac{r}{4}\sin(2r) + 0.75r^2$. Here, Γ is a parameter known as the vortex intensity, r denotes the distance from the core of the vortex, and ω is an angular wave frequency specifying the width of the vortex. The Mach number ε is controlled by adjusting the value of ζ via the relation $\varepsilon = 0.1\zeta/\sqrt{110}$. We further assume the gas law $p(\rho) = \rho^2$. We take a mesh grid of 100×100 points and impose periodic boundary conditions on all sides. In order to assess the dissipation of the scheme and its dependence on ε , we compute the flow Mach number $M = \sqrt{(u - 0.1)^2 + v^2}/c$ at one period of rotation $T = 5/3$ for different values $\varepsilon = 10^{-1}, 10^{-2}, 10^{-3}, 10^{-4}, 10^{-5}, 10^{-6}$. We present the pseudocolour plots of the Mach number in Figure 7 which clearly shows the independence of M on ε compared to the initial Mach number distribution given in Figure 6. In order to further elucidate the idea, in Figure 8 we plot the cross-section of the vorticity along the x -axis for the chosen values of ε after one period of time and the plot of the relative kinetic energies. It is evident that the vorticity distributions remain independent of ε and the dissipation in relative kinetic energy is only 0.07%. For this test problem, we note that $\eta \sim 0.013$.

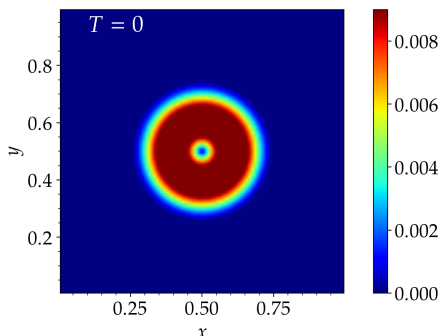


FIGURE 6. Pseudocolour plot of the Mach number at time $T = 0$.

7.4. Cylindrical Explosion. Here we consider a 2D cylindrical explosion problem from [19] with the isothermal pressure law $p(\rho) = \rho$, and the purpose of this case study is twofold. First, we want to illustrate the shock capturing capabilities of the present scheme in compressible regimes ($\varepsilon = 1$) and second, its ability to capture the incompressible limit when $\varepsilon \rightarrow 0$. The initial density reads

$$\rho(0, x, y) = \begin{cases} 1 + \varepsilon^2, & \text{if } r^2 \leq \frac{1}{4}, \\ 1, & \text{otherwise,} \end{cases}$$

where $r = \sqrt{x^2 + y^2}$. The initial velocity field is taken as

$$(u, v)(0, x, y) = -\frac{\alpha(x, y)}{\rho(0, x, y)} \left(\frac{x}{r}, \frac{y}{r} \right) \mathcal{X}_{r > 10^{-15}},$$

where $\alpha(x, y) = \max\{0, 1 - r\}(1 - e^{-16r^2})$. We consider the computational domain $[-1, 1] \times [-1, 1]$ and take 100×100 grid points. The boundaries are periodic everywhere. In Figure 9 we present the

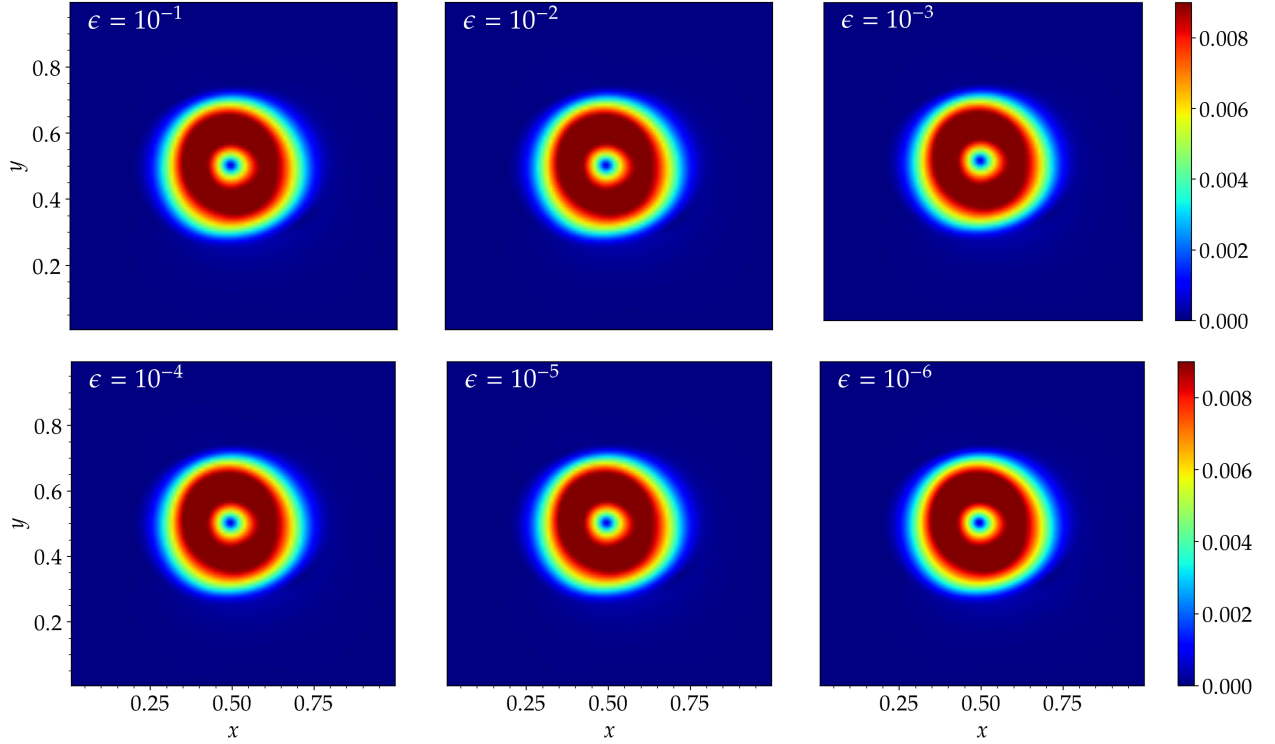


FIGURE 7. Pseudocolour plots of the Mach number at time $T = 5/3$ for $\varepsilon = 10^{-1}, 10^{-2}, 10^{-3}, 10^{-4}, 10^{-5}, 10^{-6}$.

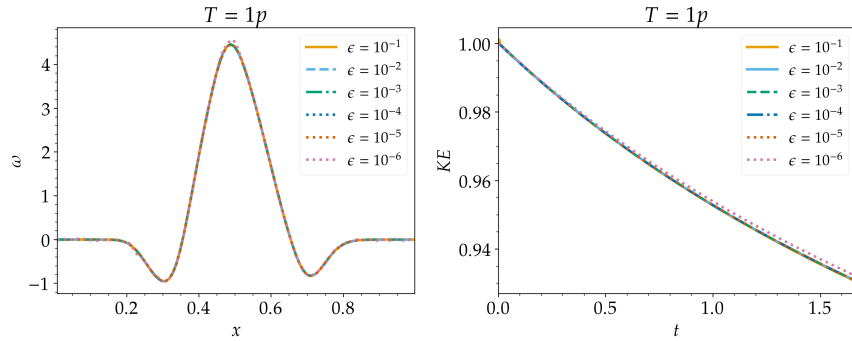


FIGURE 8. Cross-sections of the vorticity (left) and relative kinetic energy (right) for $\varepsilon = 10^{-1}, 10^{-2}, 10^{-3}, 10^{-4}, 10^{-5}, 10^{-6}$.

surface plots of the density which clearly indicates the scheme's shock capturing capabilities. Also, we compare an 1D cut along the x -direction of the cylindrically symmetric density profile with a reference solution obtained by an explicit Rusanov scheme with mesh resolution $\Delta x = 1/500$, $\Delta t = 1/10000$ to validate the correctness of the shock speed. Furthermore, since the problem is cylindrically symmetric, we compare the radial velocity with the quasi-exact reference solution obtained by the 1D Euler equations in radial coordinates [58] on 200 mesh points in Figure 10.

Finally, in Figure 11 we give the surface plot of the density deviation from the constant state 1 computed at time $T = 0.05$ in the incompressible regime for $\varepsilon = 10^{-4}$. We clearly note that the

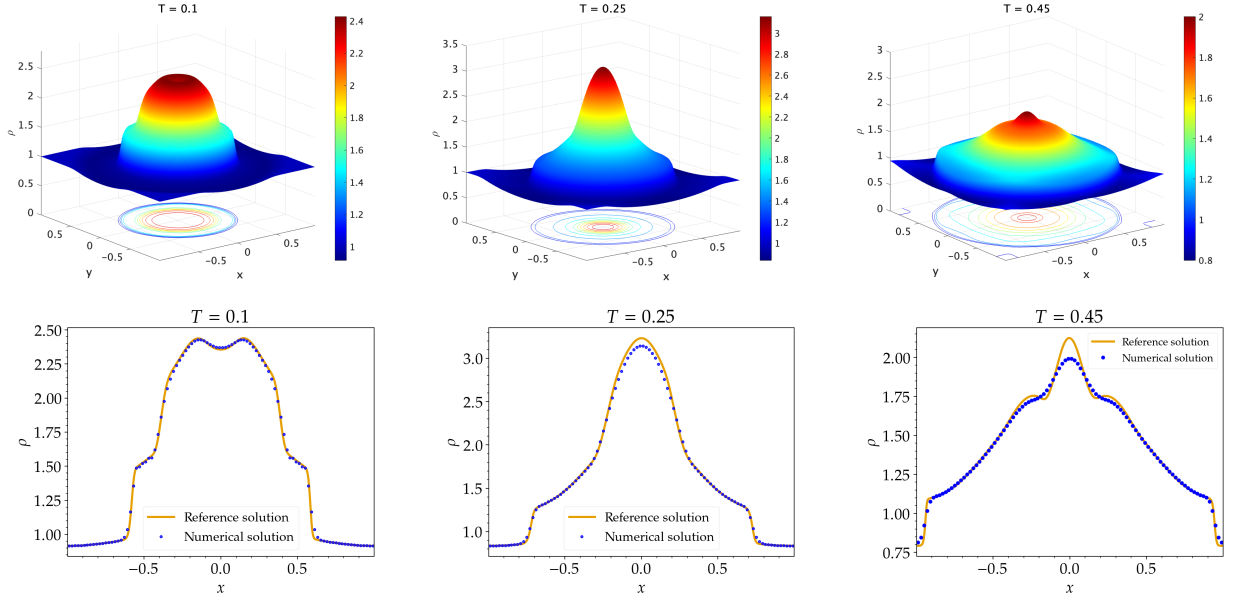


FIGURE 9. Surface plots of the density (top) and comparison of cuts along the x -direction (bottom) for the cylindrical explosion problem at times $T = 0.1, 0.25, 0.45$ for $\varepsilon = 1$.

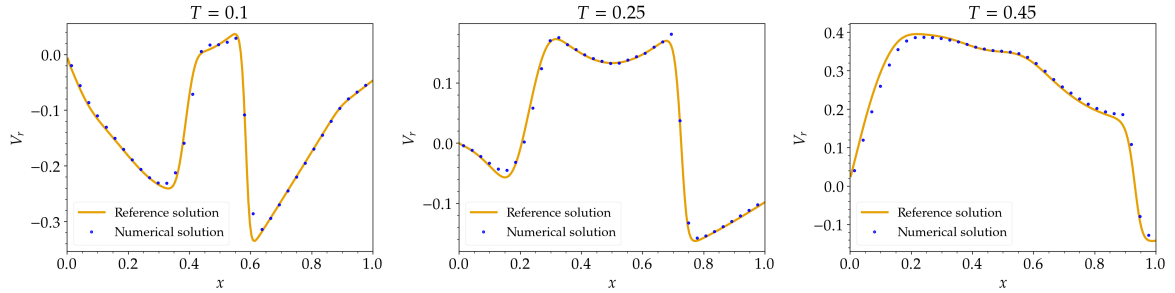


FIGURE 10. 1D cuts of the radial velocity compared to a quasi-exact radial solution for the cylindrical explosion problem at times $T = 0.1, 0.25, 0.45$ for $\varepsilon = 1$.

numerical solution has converged to a constant density $\rho = 1$ with an error 10^{-9} and the divergence errors are of the order 10^{-4} . The minimum and maximum values of η observed for this problem are 1.5 and 6.6, respectively.

7.5. Incompressible Problem. We consider the following incompressible initial data from [22] wherein

$$\rho(0, x, y) = 1, \quad u(0, x, y) = -\sin x \cos y, \quad v(0, x, y) = \cos x \sin y.$$

The pressure law is taken as $p(\rho) = \rho^2$. For this problem an exact solution is available. We take the computational domain $[0, 2\pi] \times [0, 2\pi]$ which is divided into 32×32 mesh points. In Figure 12 we compare the exact vorticity and the numerical vorticity at time $T = 2$ for $\varepsilon = 0.01$. The figure clearly indicates the convergence of the numerical solution to the incompressible solution even on a coarse mesh. In Table 1 the relative errors between the exact and computed vorticities along with

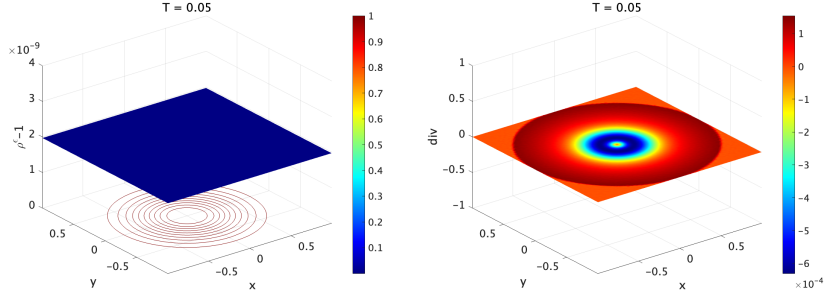


FIGURE 11. Surface plots of the deviation of density from 1 and the divergence of the velocity for the cylindrical explosion problem at time $T = 0.05$ for $\varepsilon = 10^{-4}$.

the rates of convergence are tabulated. We clearly notice first order convergence in all three norms L^1 , L^2 and L^∞ . We observe $\eta \sim 1.5$ for this test case.

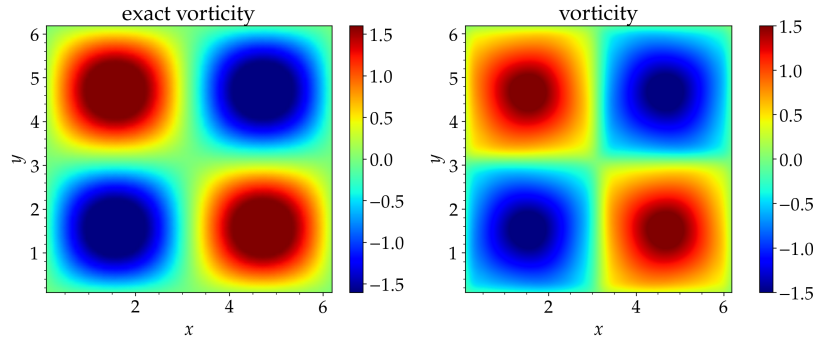


FIGURE 12. Comparison of the exact and numerical vorticity for the incompressible problem for $\varepsilon = 0.01$ at time $T = 2$.

Grid	L^1 error	Rate	L^2 error	Rate	L^∞ error	Rate
16×16	0.306722	-	0.323460	-	0.374421	-
32×32	0.190525	0.68688	0.192703	0.747172	0.202888	0.883933
64×64	0.120086	0.665848	0.114076	0.756426	0.111018	0.869871
128×128	0.068017	0.820077	0.063206	0.851839	0.058597	0.921893
256×256	0.036152	0.911807	0.033302	0.924480	0.030259	0.953451

TABLE 1. The relative errors in vorticity and rates of convergence for the incompressible problem in L^1 , L^2 and L^∞ norms for $\varepsilon = 0.01$.

7.6. Shear Flow Problem. We consider the shear flow problem from [22] with the following initial data:

$$\rho(0, x, y) = \pi/15, \quad u(0, x, y) = \begin{cases} \tanh \frac{y-\pi/2}{\pi/15}, & \text{if } y \leq \pi, \\ \tanh \frac{3\pi-y}{\pi/15}, & \text{if } y > \pi, \end{cases} \quad v(0, x, y) = 0.05 \sin x.$$

The goal of this test problem is two-fold. First, we show the convergence of the numerical densities to the constant incompressible density as $\varepsilon \rightarrow 0$. To this end, we calculate the differences between

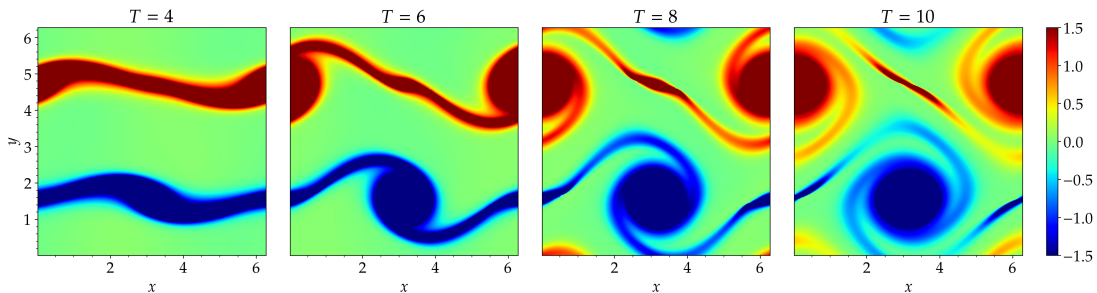


FIGURE 13. Vorticity for $\varepsilon = 10^{-6}$ at times $T = 4, 6, 8$ and 10 for the shear flow problem.

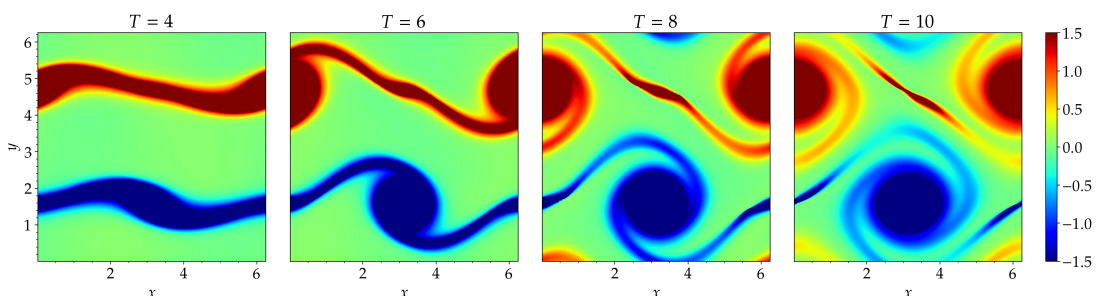


FIGURE 14. Vorticity at times $T = 4, 6, 8, 10$ for the shear flow problem computed using the limiting scheme (6.9)-(6.10).

the computed density and the constant value $\pi/15$ in L^2 -norm and tabulate them against ε in Table 2. We notice that the errors decay as $\mathcal{O}(\varepsilon^2)$ as $\varepsilon \rightarrow 0$ in accordance with the theoretical results [43]. Second, in order to establish numerically the AP property, we simulate this problem in an incompressible regime by setting a very small value $\varepsilon = 10^{-6}$. The computational domain $[0, 2\pi] \times [0, 2\pi]$ is divided into 256×256 mesh points. The plots of the vorticity obtained using the present scheme and the one computed using the numerical solution of the limiting incompressible scheme (6.9)-(6.10) at times $T = 4, 6, 8, 10$ are presented in Figure 13 and Figure 14, respectively. The plots clearly show that the scheme can resolve complex vortex structures of the incompressible flow very well and the numerical solution is indistinguishable from that of the limiting scheme. The value $\eta \sim 7.16$ is observed for this test case.

ε	10^{-1}	10^{-2}	10^{-3}	10^{-4}	10^{-5}	10^{-6}
$\ \rho^\varepsilon - \pi/15\ _{L^2} = 0.6 \times$	10^{-2}	10^{-4}	10^{-6}	10^{-8}	10^{-10}	10^{-12}

TABLE 2. The L^2 errors in density for the shear flow problem.

8. CONCLUDING REMARKS

An AP and entropy stable scheme for the barotropic Euler system in the zero Mach number limit is designed, analysed and implemented. The entropy stability is achieved by introducing a velocity shift proportional to the pressure gradient in the convective fluxes, which is responsible for the dissipation of mechanical energy. The numerical scheme obtained by using semi-implicit in time and upwind in space finite volume discretisations, possesses several attractive features: the

positivity of density, the entropy stability and the consistency with continuous equations when the grid parameters go to zero. The scheme is stable under a CFL condition which permits large time-steps at low Mach numbers. The apriori entropy stability estimate leads to a bound on the second order pressure which in turn allows the passage to the zero Mach number limit to get a consistent, velocity stabilised scheme for the incompressible limit system. The results of numerical case studies clearly validate the positivity preservation, the correct shock capturing capabilities in the compressible regimes, the ability to simulate weakly compressible flows even for ill-prepared initial data and the AP property in the zero Mach number limit with exact convergence rates with respect to the vanishing Mach number. Numerical experiments indicate a first order convergence for the scheme.

DATA AVAILABILITY AND DECLARATION

Enquiries about data availability should be directed to the authors. The authors declare to have no conflict of interest.

REFERENCES

- [1] K. R. Arun, A. J. Das Gupta, and S. Samantaray. Analysis of an asymptotic preserving low Mach number accurate IMEX-RK scheme for the wave equation system. *Appl. Math. Comput.*, 411:Paper No. 126469, 20, 2021.
- [2] K. R. Arun, M. Krishnan, and S. Samantaray. A unified asymptotic preserving and well-balanced scheme for the Euler system with multiscale relaxation. *Comput. & Fluids*, 233:Paper No. 105248, 13, 2022.
- [3] K. R. Arun and S. Samantaray. Asymptotic preserving low Mach number accurate IMEX finite volume schemes for the isentropic Euler equations. *J. Sci. Comput.*, 82(2):Art. 35, 32, 2020.
- [4] A. Bermúdez, S. Busto, M. Dumbser, J. L. Ferrín, L. Saavedra, and M. E. Vázquez-Cendón. A staggered semi-implicit hybrid FV/FE projection method for weakly compressible flows. *J. Comput. Phys.*, 421:109743, 31, 2020.
- [5] H. Bijl and P. Wesseling. A unified method for computing incompressible and compressible flows in boundary-fitted coordinates. *J. Comput. Phys.*, 141(2):153–173, 1998.
- [6] G. Bispen, K. R. Arun, M. Lukáčová-Medvid’ová, and S. Noelle. IMEX large time step finite volume methods for low Froude number shallow water flows. *Commun. Comput. Phys.*, 16(2):307–347, 2014.
- [7] S. Boscarino, J.-M. Qiu, G. Russo, and T. Xiong. A high order semi-implicit IMEX WENO scheme for the all-Mach isentropic Euler system. *J. Comput. Phys.*, 392:594–618, 2019.
- [8] S. Boscarino, G. Russo, and L. Scandurra. All Mach number second order semi-implicit scheme for the Euler equations of gas dynamics. *J. Sci. Comput.*, 77(2):850–884, 2018.
- [9] S. Busto, L. Río-Martín, M. E. Vázquez-Cendón, and M. Dumbser. A semi-implicit hybrid finite volume/finite element scheme for all Mach number flows on staggered unstructured meshes. *Appl. Math. Comput.*, 402:Paper No. 126117, 29, 2021.
- [10] S. Busto, M. Tavelli, W. Boscheri, and M. Dumbser. Efficient high order accurate staggered semi-implicit discontinuous Galerkin methods for natural convection problems. *Comput. & Fluids*, 198:104399, 28, 2020.
- [11] C. Chalons, M. Girardin, and S. Kokh. An all-regime Lagrange-projection like scheme for the gas dynamics equations on unstructured meshes. *Commun. Comput. Phys.*, 20(1):188–233, 2016.
- [12] A. J. Chorin. Numerical solution of the Navier-Stokes equations. *Math. Comp.*, 22:745–762, 1968.
- [13] P. G. Ciarlet. Basic error estimates for elliptic problems. In *Handbook of numerical analysis, Vol. II*, Handb. Numer. Anal., II, pages 17–351. North-Holland, Amsterdam, 1991.
- [14] P. Colella and K. Pao. A projection method for low speed flows. *J. Comput. Phys.*, 149(2):245–269, 1999.
- [15] F. Couderc, A. Duran, and J.-P. Vila. An explicit asymptotic preserving low Froude scheme for the multilayer shallow water model with density stratification. *J. Comput. Phys.*, 343:235–270, 2017.
- [16] P. Degond and M. Tang. All speed scheme for the low Mach number limit of the isentropic Euler equations. *Commun. Comput. Phys.*, 10(1):1–31, 2011.
- [17] K. Deimling. *Nonlinear functional analysis*. Springer-Verlag, Berlin, 1985.
- [18] S. Dellacherie. Analysis of Godunov type schemes applied to the compressible Euler system at low Mach number. *J. Comput. Phys.*, 229(4):978–1016, 2010.
- [19] G. Dimarco, R. Loubère, and M.-H. Vignal. Study of a new asymptotic preserving scheme for the Euler system in the low Mach number limit. *SIAM J. Sci. Comput.*, 39(5):A2099–A2128, 2017.

- [20] A. Duran, J.-P. Vila, and R. Baraille. Semi-implicit staggered mesh scheme for the multi-layer shallow water system. *C. R. Math. Acad. Sci. Paris*, 355(12):1298–1306, 2017.
- [21] A. Duran, J.-P. Vila, and R. Baraille. Energy-stable staggered schemes for the Shallow Water equations. *J. Comput. Phys.*, 401:109051, 24, 2020.
- [22] W. E and C.-W. Shu. A numerical resolution study of high order essentially non-oscillatory schemes applied to incompressible flow. *J. Comput. Phys.*, 110(1):39–46, 1994.
- [23] A. Ern and J.-L. Guermond. *Theory and practice of finite elements*, volume 159 of *Applied Mathematical Sciences*. Springer-Verlag, New York, 2004.
- [24] R. Eymard, T. Gallouët, M. Ghilani, and R. Herbin. Error estimates for the approximate solutions of a nonlinear hyperbolic equation given by finite volume schemes. *IMA J. Numer. Anal.*, 18(4):563–594, 1998.
- [25] T. Gallouët, R. Herbin, and J.-C. Latché. $W^{1,q}$ stability of the Fortin operator for the MAC scheme. *Calcolo*, 49(1):63–71, 2012.
- [26] T. Gallouët, R. Herbin, and J.-C. Latché. On the weak consistency of finite volumes schemes for conservation laws on general meshes. *SeMA J.*, 76(4):581–594, 2019.
- [27] T. Gallouët, R. Herbin, and J.-C. Latché. Lax–Wendroff consistency of finite volume schemes for systems of non linear conservation laws: extension to staggered schemes. *SeMA J.*, 79(2):333–354, 2022.
- [28] T. Gallouët, R. Herbin, J.-C. Latché, and K. Malle. Convergence of the marker-and-cell scheme for the incompressible Navier-Stokes equations on non-uniform grids. *Found. Comput. Math.*, 18(1):249–289, 2018.
- [29] T. Gallouët, R. Herbin, D. Maltese, and A. Novotny. Error estimates for a numerical approximation to the compressible barotropic Navier-Stokes equations. *IMA J. Numer. Anal.*, 36(2):543–592, 2016.
- [30] T. Gallouët, D. Maltese, and A. Novotny. Error estimates for the implicit MAC scheme for the compressible Navier-Stokes equations. *Numer. Math.*, 141(2):495–567, 2019.
- [31] L. Gastaldo, R. Herbin, J.-C. Latché, and N. Therme. A MUSCL-type segregated–explicit staggered scheme for the Euler equations. *Comput. & Fluids*, 175:91–110, 2018.
- [32] N. Grenier, J.-P. Vila, and P. Villedieu. An accurate low-Mach scheme for a compressible two-fluid model applied to free-surface flows. *J. Comput. Phys.*, 252:1–19, 2013.
- [33] H. Guillard and C. Viozat. On the behaviour of upwind schemes in the low Mach number limit. *Comput. & Fluids*, 28(1):63–86, 1999.
- [34] J. Haack, S. Jin, and J.-G. Liu. An all-speed asymptotic-preserving method for the isentropic Euler and Navier-Stokes equations. *Commun. Comput. Phys.*, 12(4):955–980, 2012.
- [35] F. H. Harlow and A. A. Amsden. Numerical calculation of almost incompressible flow. *J. Comput. Phys.*, 3(1):80–93, 1968.
- [36] F. H. Harlow and J. E. Welch. Numerical calculation of time-dependent viscous incompressible flow of fluid with free surface. *Phys. Fluids*, 8(12):2182–2189, 1965.
- [37] R. Herbin, W. Kheriji, and J.-C. Latché. On some implicit and semi-implicit staggered schemes for the shallow water and Euler equations. *ESAIM Math. Model. Numer. Anal.*, 48(6):1807–1857, 2014.
- [38] R. Herbin, J.-C. Latché, Y. Nasser, and N. Therme. A consistent quasi-second-order staggered scheme for the two-dimensional shallow water equations. *IMA J. Numer. Anal.*, 43(1):99–143, 2023.
- [39] R. Herbin, J.-C. Latché, and K. Saleh. Low Mach number limit of some staggered schemes for compressible barotropic flows. *Math. Comp.*, 90(329):1039–1087, 2021.
- [40] R. I. Issa, A. D. Gosman, and A. P. Watkins. The computation of compressible and incompressible recirculating flows by a noniterative implicit scheme. *J. Comput. Phys.*, 62(1):66–82, 1986.
- [41] S. Jin. Efficient asymptotic-preserving (AP) schemes for some multiscale kinetic equations. *SIAM J. Sci. Comput.*, 21(2):441–454, 1999.
- [42] K. C. Karki and S. V. Patankar. Pressure based calculation procedure for viscous flows at all speeds in arbitrary configurations. *AIAA Journal*, 27(9):1167–1174, 1989.
- [43] S. Klainerman and A. Majda. Compressible and incompressible fluids. *Comm. Pure Appl. Math.*, 35(5):629–651, 1982.
- [44] R. Klein. Semi-implicit extension of a Godunov-type scheme based on low Mach number asymptotics. I. One-dimensional flow. *J. Comput. Phys.*, 121(2):213–237, 1995.
- [45] N. Kwatra, J. Su, J. T. Grétarsson, and R. Fedkiw. A method for avoiding the acoustic time step restriction in compressible flow. *J. Comput. Phys.*, 228(11):4146–4161, 2009.
- [46] P.-L. Lions and N. Masmoudi. Incompressible limit for a viscous compressible fluid. *J. Math. Pures Appl. (9)*, 77(6):585–627, 1998.
- [47] Y. Moguen, T. Kousksou, P. Bruel, J. Vierendeels, and E. Dick. Pressure-velocity coupling allowing acoustic calculation in low Mach number flow. *J. Comput. Phys.*, 231(16):5522–5541, 2012.

- [48] C.-D. Munz, S. Roller, R. Klein, and K. J. Geratz. The extension of incompressible flow solvers to the weakly compressible regime. *Comput. & Fluids*, 32(2):173–196, 2003.
- [49] L. Nirenberg. *Topics in nonlinear functional analysis*, volume 6 of *Courant Lecture Notes in Mathematics*. New York University, Courant Institute of Mathematical Sciences, New York; American Mathematical Society, Providence, RI, 2001. Chapter 6 by E. Zehnder, Notes by R. A. Artino, Revised reprint of the 1974 original.
- [50] S. Noelle, G. Bispen, K. R. Arun, M. Lukáčová-Medvidová, and C.-D. Munz. A weakly asymptotic preserving low Mach number scheme for the Euler equations of gas dynamics. *SIAM J. Sci. Comput.*, 36(6):B989–B1024, 2014.
- [51] D. O’Regan, Y. J. Cho, and Y.-Q. Chen. *Topological degree theory and applications*, volume 10 of *Series in Mathematical Analysis and Applications*. Chapman & Hall/CRC, Boca Raton, FL, 2006.
- [52] M. Parisot and J.-P. Vila. Centered-potential regularization for the advection upstream splitting method. *SIAM J. Numer. Anal.*, 54(5):3083–3104, 2016.
- [53] J. H. Park and C.-D. Munz. Multiple pressure variables methods for fluid flow at all Mach numbers. *Internat. J. Numer. Methods Fluids*, 49(8):905–931, 2005.
- [54] S. Schochet. Fast singular limits of hyperbolic PDEs. *J. Differential Equations*, 114(2):476–512, 1994.
- [55] D. Shin and J. C. Strikwerda. Inf-sup conditions for finite-difference approximations of the Stokes equations. *J. Austral. Math. Soc. Ser. B*, 39(1):121–134, 1997.
- [56] M. Tavelli and M. Dumbser. A pressure-based semi-implicit space–time discontinuous galerkin method on staggered unstructured meshes for the solution of the compressible navier–stokes equations at all mach numbers. *Journal of Computational Physics*, 341:341–376, jul 2017.
- [57] A. Thomann, G. Puppo, and C. Klingenberg. An all speed second order well-balanced IMEX relaxation scheme for the Euler equations with gravity. *J. Comput. Phys.*, 420:109723, 25, 2020.
- [58] E. F. Toro. *Riemann solvers and numerical methods for fluid dynamics*. Springer-Verlag, Berlin, third edition, 2009. A practical introduction.
- [59] C. Wall, C. D. Pierce, and P. Moin. A semi-implicit method for resolution of acoustic waves in low Mach number flows. *J. Comput. Phys.*, 181(2):545–563, 2002.

SCHOOL OF MATHEMATICS, INDIAN INSTITUTE OF SCIENCE EDUCATION AND RESEARCH THIRUVANANTHAPURAM, THIRUVANANTHAPURAM 695551, INDIA

Email address: arun@iisertvm.ac.in, rahuldev19@iisertvm.ac.in, mainak17@iisertvm.ac.in